Electronic Supplementary Material (ESI) for Dalton Transactions.

Electronic Supporting Information

Colorimetric detection of fluoride ion by anthraimidazoledione based sensor in presence of Cu^{2+} ion

Amrita Sarkar, Sudipta Bhattacharyya and Arindam Mukherjee*

Contents

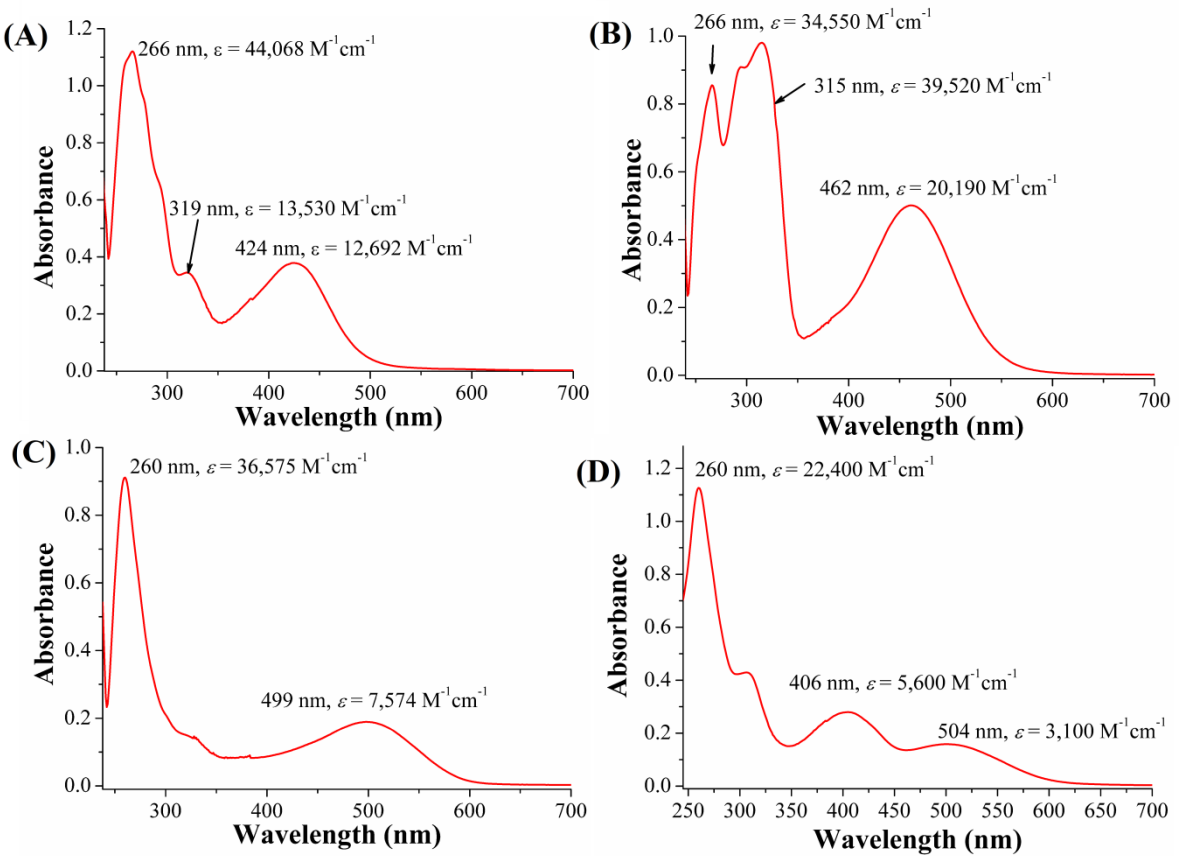

Fig. S1 UV-vis spectra of **1-4** in acetonitrile (2% DMSO). The concentration of **1-4** is 25 μM.

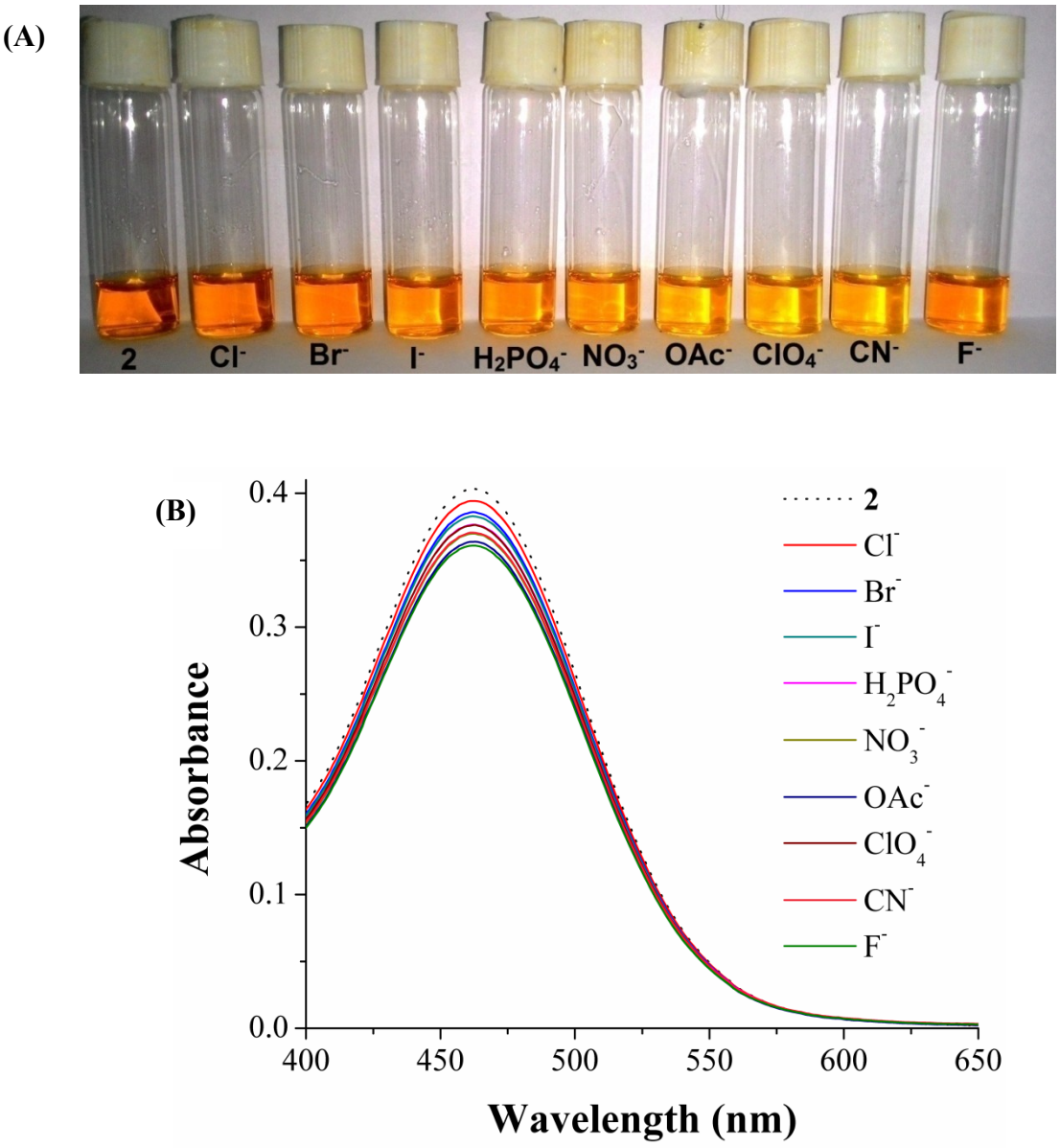

Fig. S2 (A) Colorimetric response of **2** (25 μM) in presence of different anions (1.5 X 10^{-4} M) in acetonitrile (2 % DMSO) solution. (B) UV-vis spectra of **2** (25 μM) in presence of different anions (1.5 X 10^{-4} M) in acetonitrile (2 % DMSO) solution. Charge transfer band at 462 nm is observed.

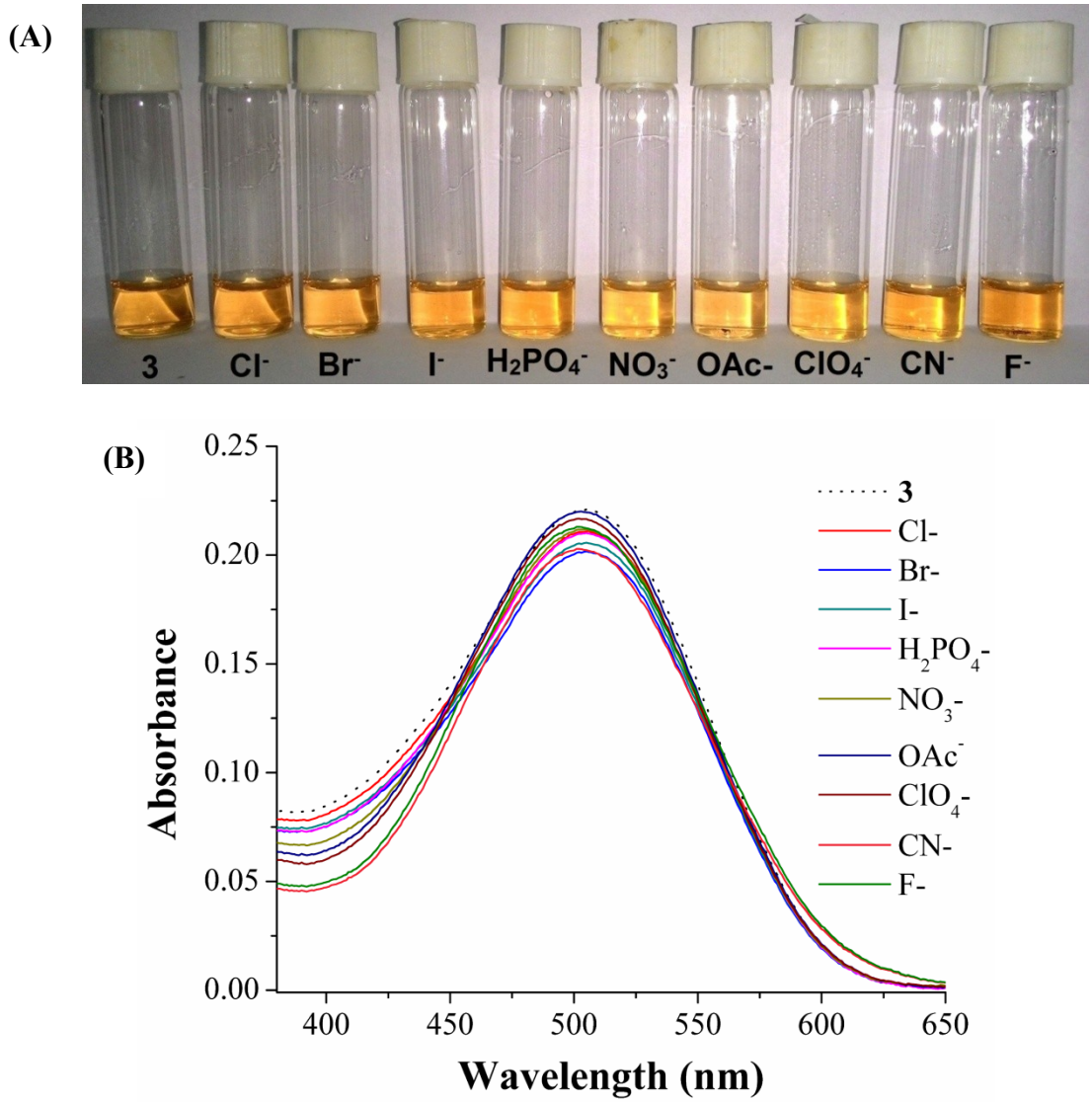

Fig. S3 (A) Colorimetric response of **3** (25 μM) in presence of different anions (1.5 X 10^{-4} M) in acetonitrile (2 % DMSO) solution. (B) UV-vis spectra of **3** (25 μM) in presence of different anions (1.5 X 10^{-4} M) in acetonitrile (2 % DMSO) solution. Charge transfer band at 500 nm is observed.

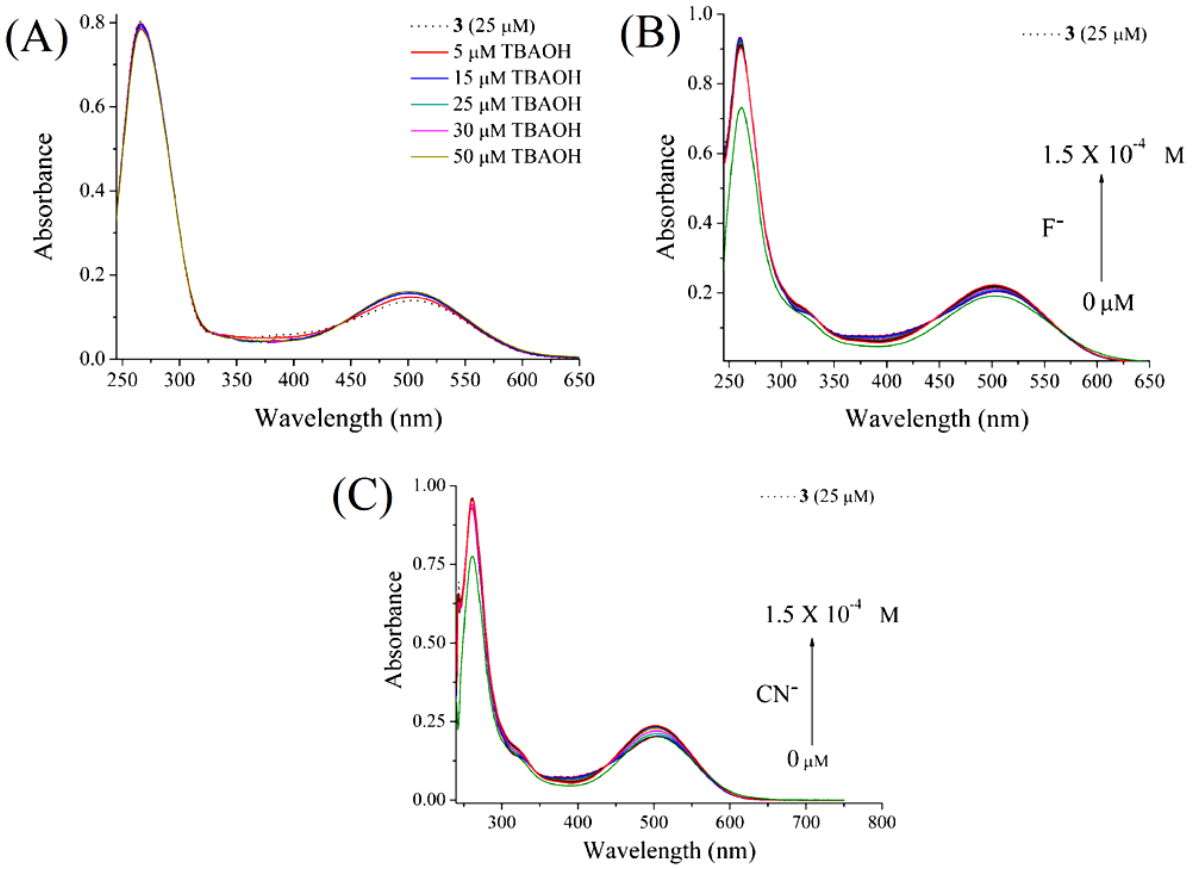

Fig. S4 (A) UV-vis titration of **3** in acetonitrile (2% DMSO) with gradual addition of 4 μL TBAOH (1 X 10^{-3} M) solution in acetonitrile. The spectrum shows no red shift of CT band at 500 nm of **3** even after 50 μM addition of TBAOH. (B) UV-vis titration of **3** in acetonitrile (2% DMSO) with gradual addition of 4 μL TBAF (1 × 10^{-3} M) solution in acetonitrile. The highest concentration of F^- achieved was 1.5 × 10^{-4} M. The spectrum shows almost no red shift of CT band at 500 nm even after the addition of addition of 1.5 × 10^{-4} M TBAF. (C) UV-vis titration of **3** in acetonitrile (2% DMSO) with gradual addition of 4 μL TBACN (1 × 10^{-3} M) solution in acetonitrile. The highest concentration of CN^- achieved was 1.5 × 10^{-4} M. The spectrum shows almost no red shift of CT band at 500 nm even after the addition of addition of 1.5 × 10^{-4} M TBACN.

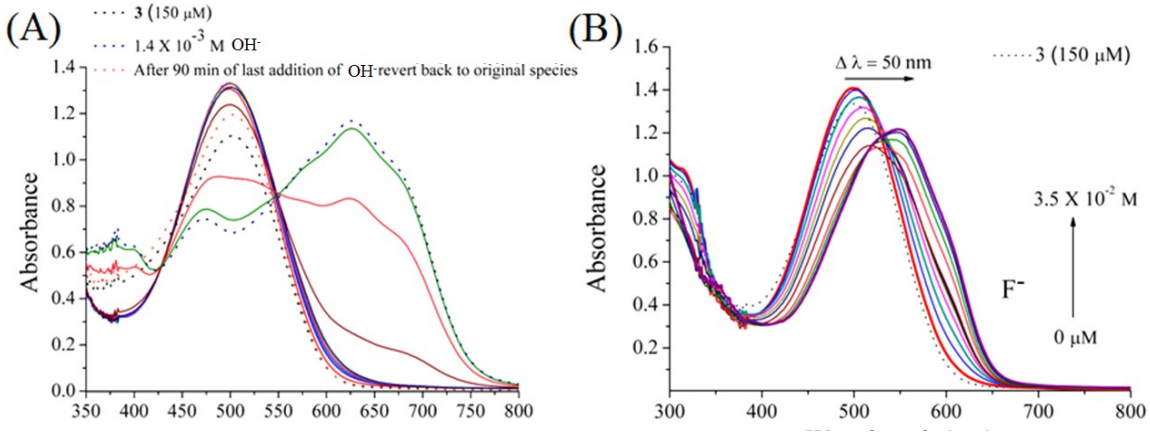

Fig. S5 (A) UV-vis titration of a higher concentration, 1.5×10^{-4} M of **3**, in acetonitrile (2% DMSO) with gradual addition of TBAOH (upto 1.4×10^{-3} M) solution in acetonitrile. The spectra shows 150 nm red shift (Δλ) after achieving saturation with the addition of 100 equivalent of OH^-. However the shifted spectra reverts back to original position after 90 min of last addidtion of OH^-. (B) UV-vis titration of **3** with much higher concentration (1.5×10^{-4} M) in acetonitrile (2% DMSO) with gradual addition of TBAF (upto 3.5×10^{-2} M) solution in acetonitrile. The spectra shows 50 nm red shift (Δλ) after achieving saturation with the addition of 234 equivalent of TBAF.

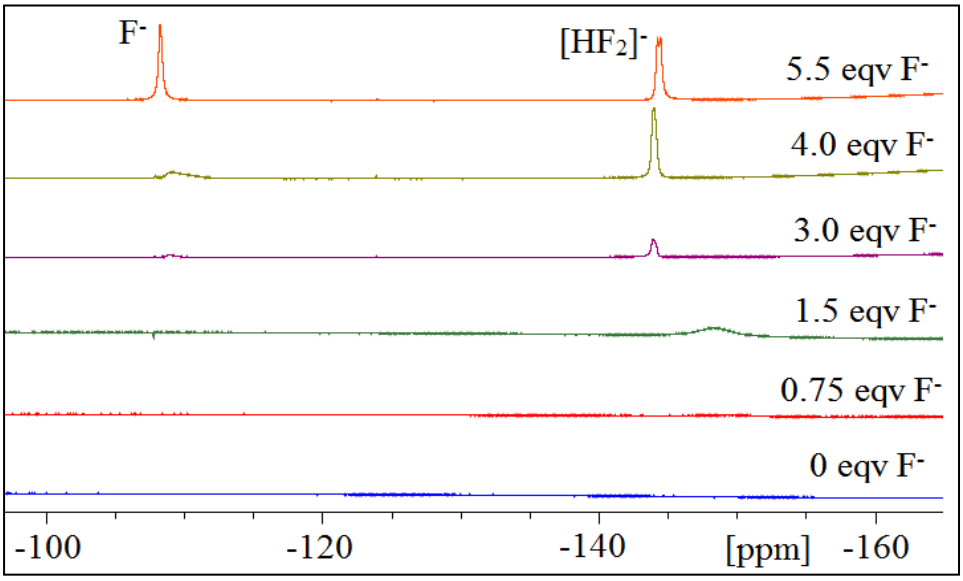

Fig. S6 ^{19}F NMR titration spectra (partial) of **1** (4.9×10^{-2} M) in DMSO-d_6 with different concentration of TBAF (given equivalent compared to **1**).

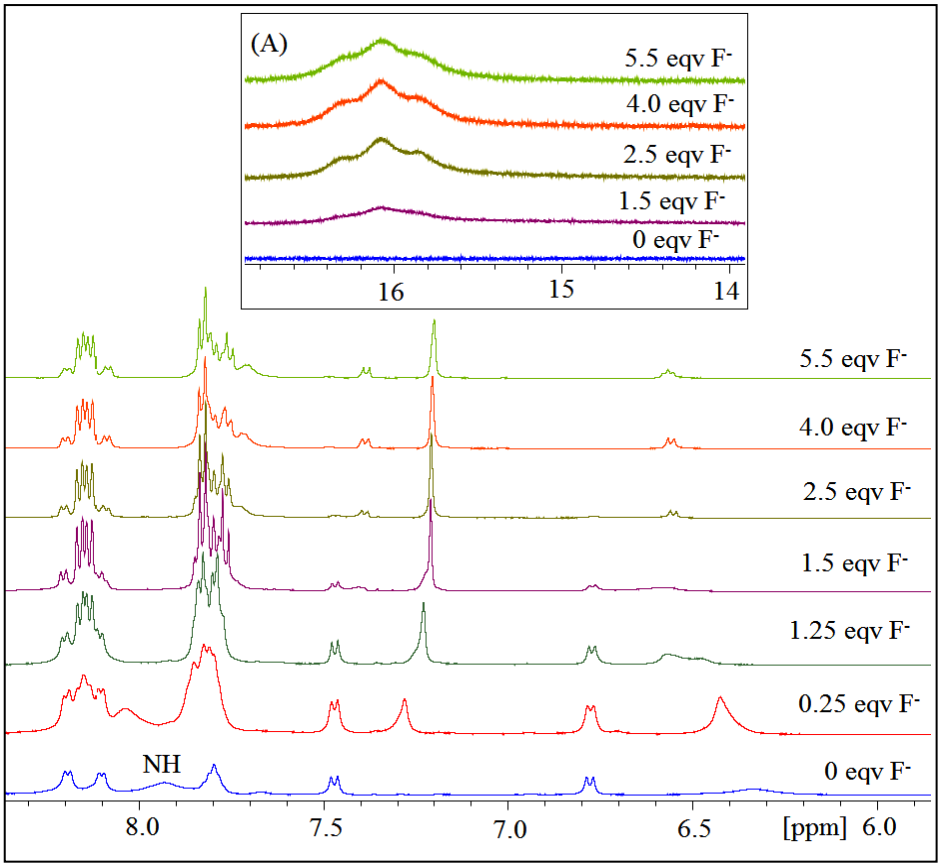

Fig. S7 Partial ^{1}H NMR spectra of **4** (9.9×10^{-2} M) in DMSO-d_6 in presence of TBAF (0-5.5 equivalent). Inset: (A) Expansion of the region 14-17 ppm in presence of 1.5 – 5.5 equivalent TBAF.

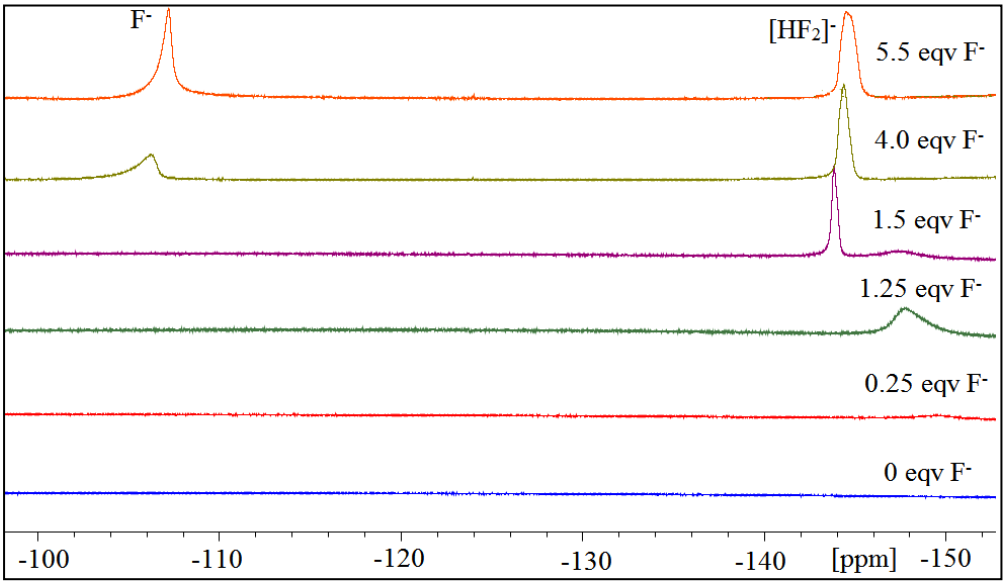

Fig. S8 ^{19}F NMR titration spectra (partial) of **4** (9.9×10^{-2} M) in DMSO-d_6 with different concentration of TBAF (given equivalent compared to **4**).

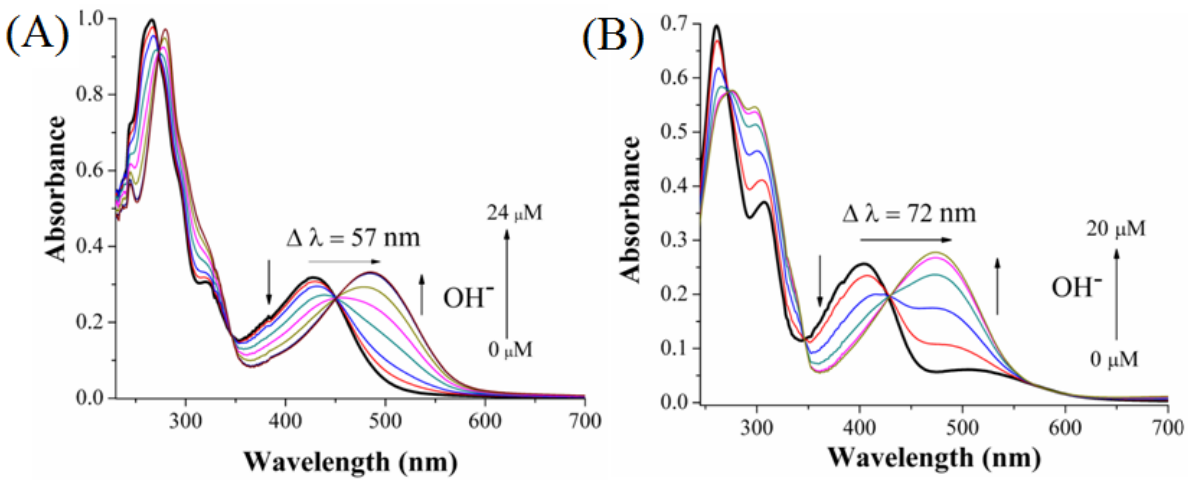

Fig. S9 UV-vis titration of **1** and **4** in acetonitrile (2% DMSO) with gradual addition of 4 μL TBAOH (1 X 10^{-3} M) solution in acetonitrile. (A) The spectral change of **1** is displayed due to addition of TBAOH. The spectra shows 57 nm red shift (Δλ) after achieving saturation with the addition of 0.96 equivalent of TBAOH. (B) The spectral change of **4** is displayed due to addition of TBAOH. The spectra shows 72 nm red shift (Δλ) after achieving saturation with the addition of 0.80 equivalent of TBAOH.

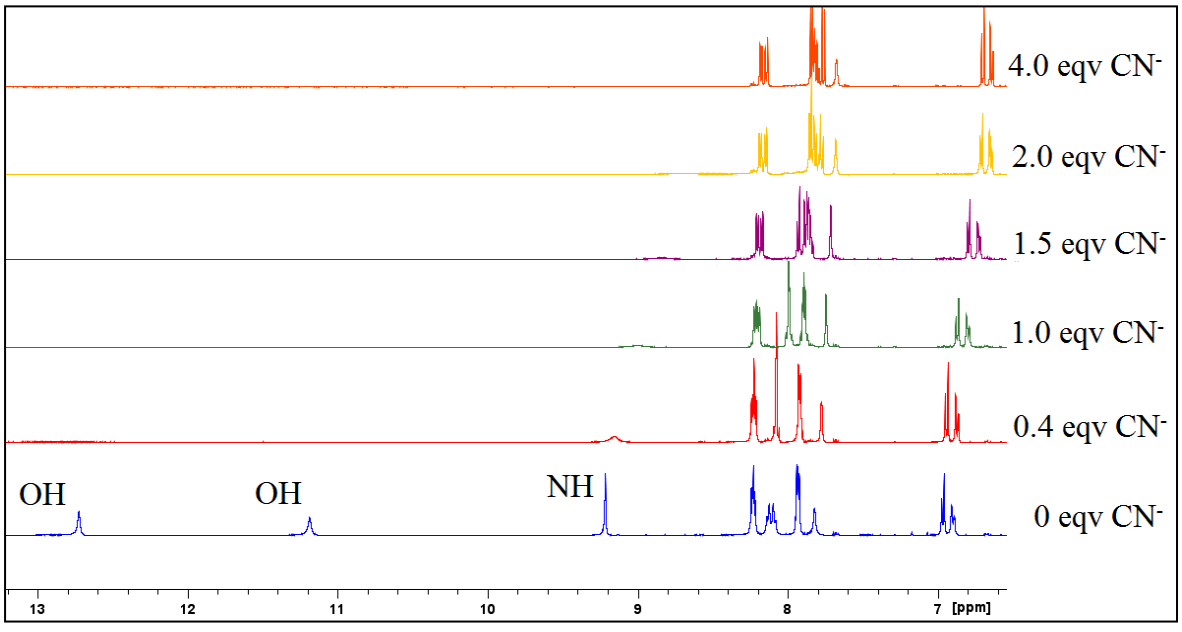

Fig. S10 Partial ^{1}H NMR spectra of **1** (4.9×10^{-2} M) in DMSO-d_6 in presence of TBACN solution (1.7×10^{-1} M) in DMSO-d_6 (0-4.0 equivalent).

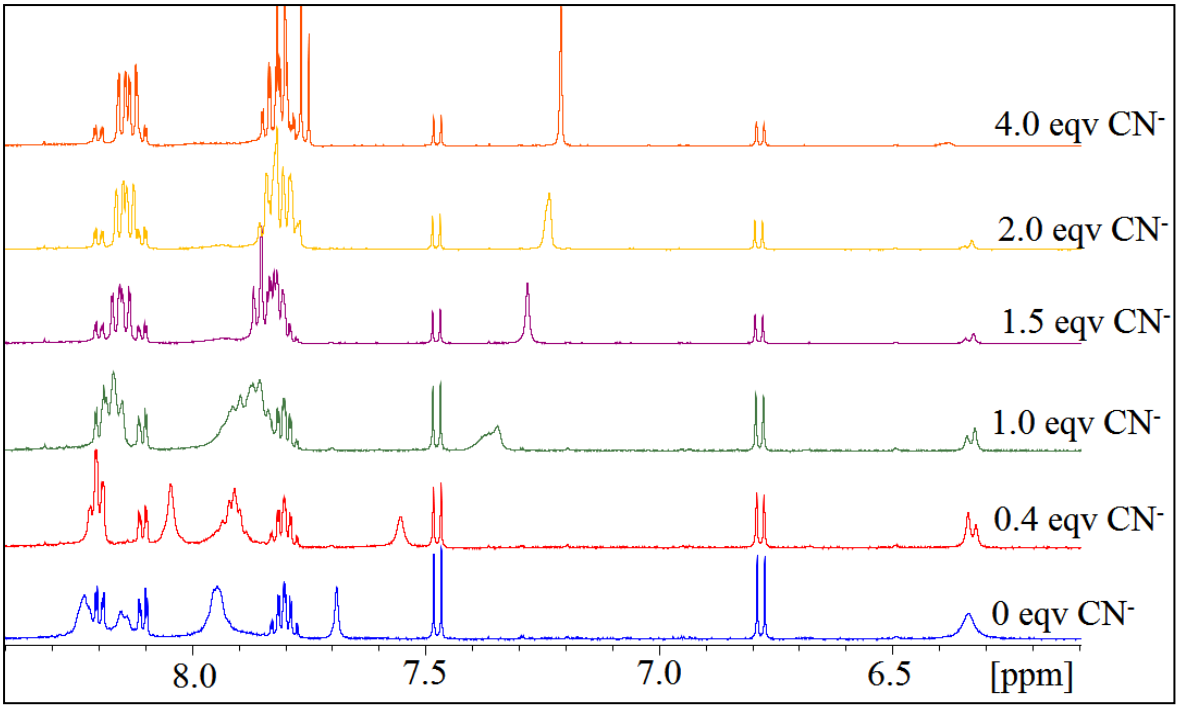

Fig. S11 Partial ^{1}H NMR spectra of **4** (7.9×10^{-2} M) in DMSO-d_6 in presence of TBACN solution (1.7×10^{-1} M) in DMSO-d_6 (0-4.0 equivalent).

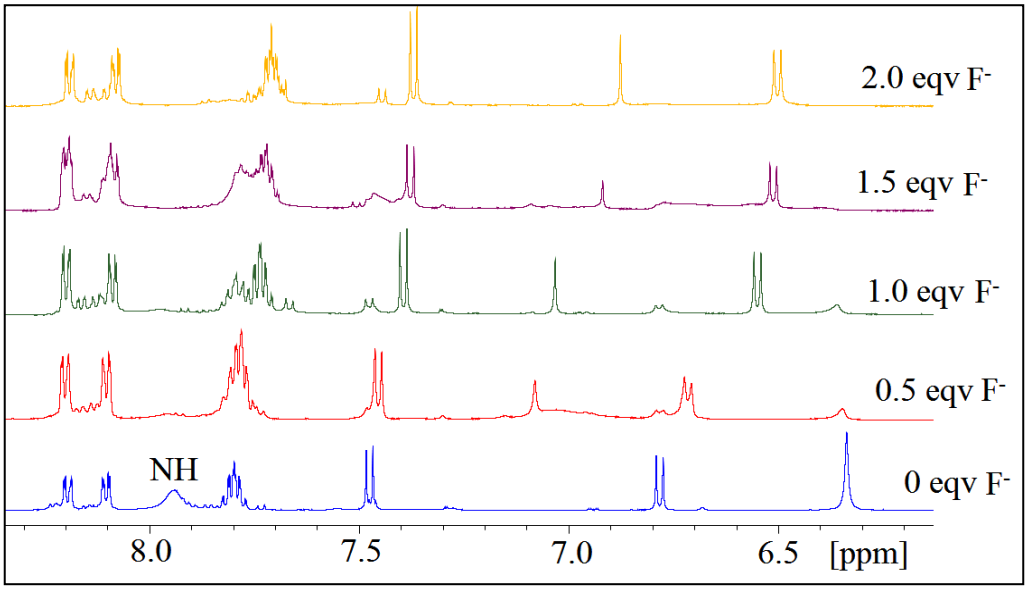

Fig. S12 Partial ^{1}H NMR spectra of **3** (concentration of **3** is 5.4×10^{-2} M) in DMSO-d_6 in presence of TBAF solution (6.75×10^{-1} M) in DMSO-d_6 (0-2.0 equivalent). Disappearance of NH peak at 7.9 ppm indicates deprotonation of imidazole hydrogen due to addition of fluoride.

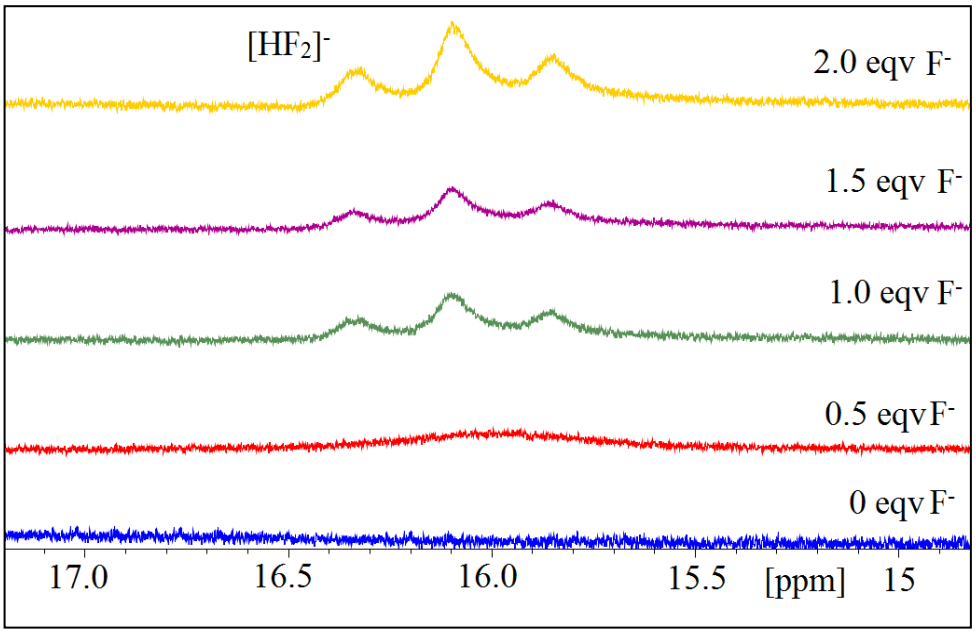

Fig. S13 Partial ^{1}H NMR spectra of **3** (concentration of **3** is 5.4 × 10^{-2} M) in DMSO-d6 in presence of TBAF solution (6.75 × 10^{-1} M) in DMSO-d_6 (0-2.0 equivalent). Formation of triplet at 16.0 ppm suggests formation of $[HF_2]^-$ adduct due to addition of fluoride.

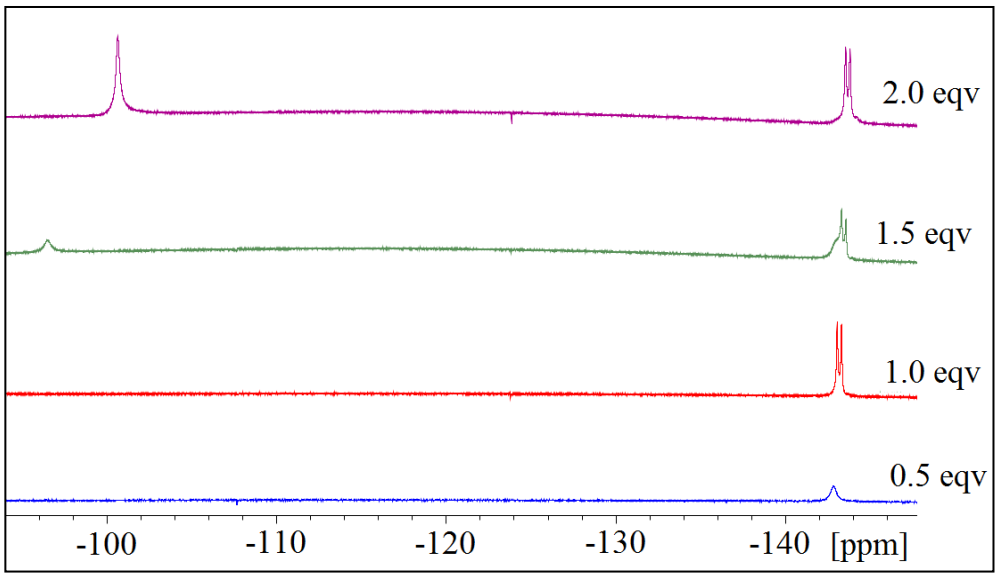

Fig. S14 Partial ^{19}F NMR spectra of **3** (concentration of **3** is 5.4 × 10^{-2} M) in DMSO-d_6 in presence of TBAF solution (6.75 × 10^{-1} M) in DMSO-d_6 (0-2.0 equivalent). Formation of doublet at -142.5 ppm suggests formation of $[HF_2]^-$ adduct due to addition of fluoride.

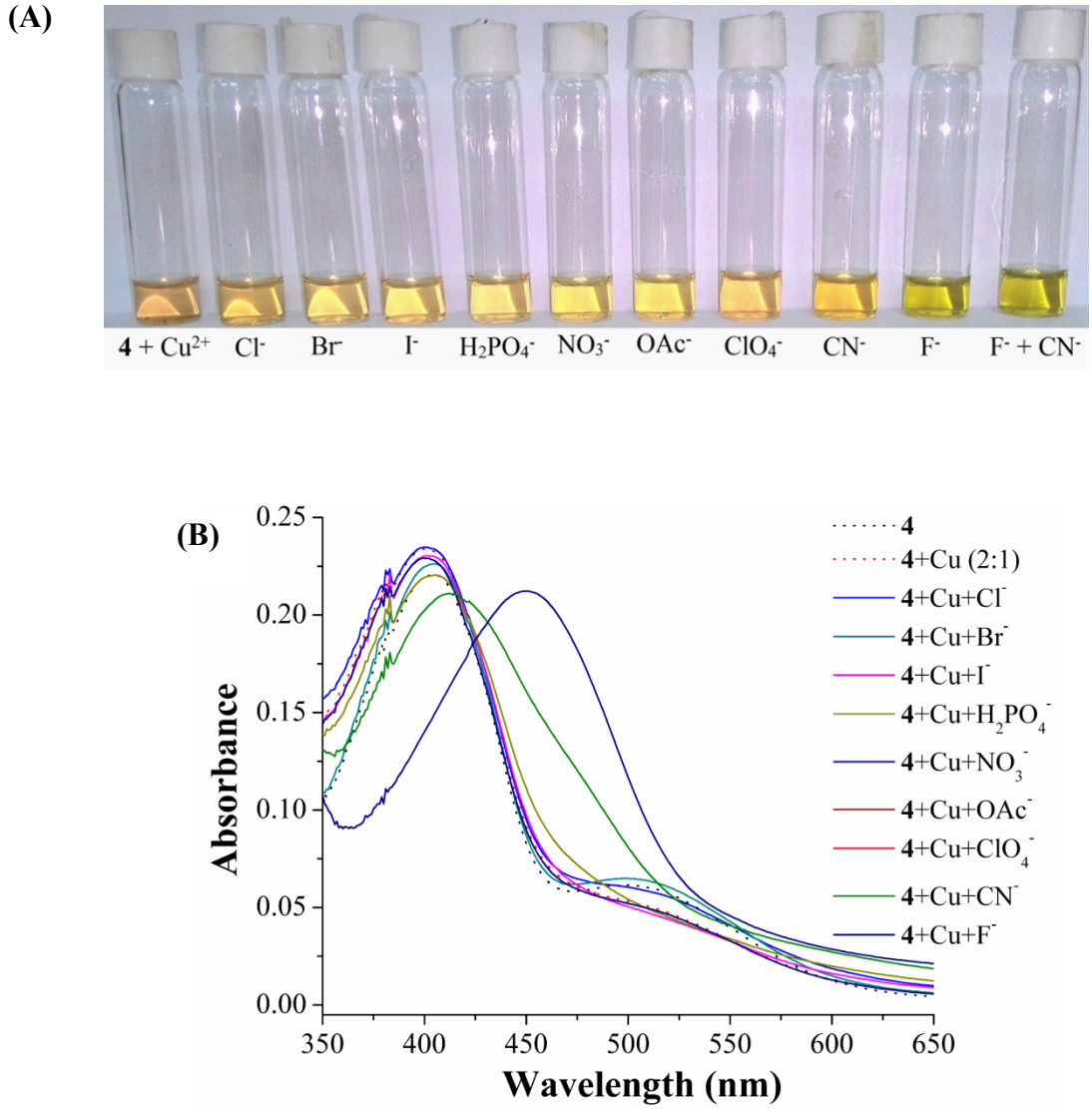

Fig. S15 (A) Colorimetric response of **4** (25 μM) in presence $CuCl_2$ (12.5 μM) with addition of different anions (1.5 X 10^{-4} M) in acetonitrile (2 % DMSO) solution. (B) UV-vis spectra of **4** (25 μM) in presence in presence $CuCl_2$ (12.5 μM) with addition of different anions (1.5 X 10^{-4} M) in acetonitrile (2 % DMSO) solution. Charge transfer band at 400 nm has been monitored.

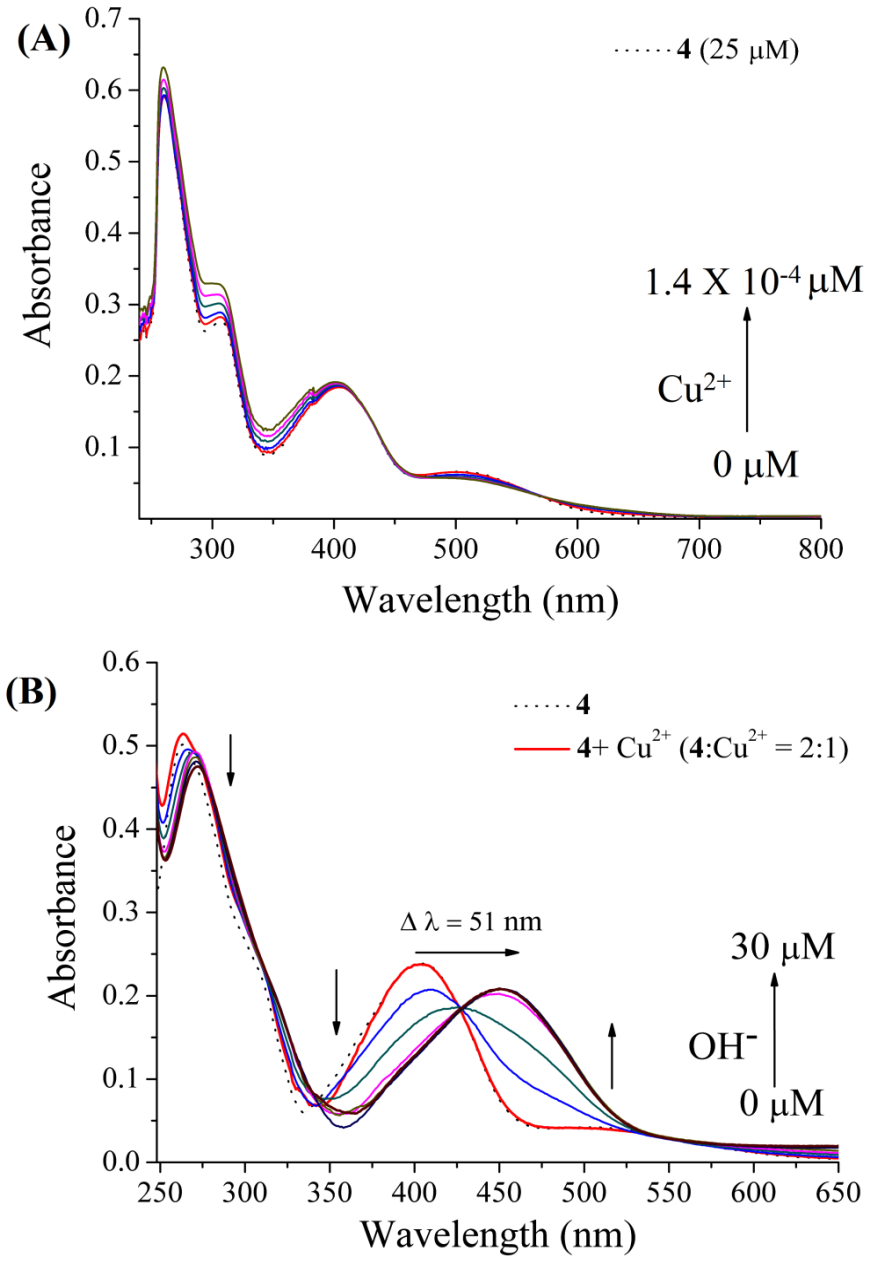

Fig. S16 (A) UV-vis titration of **4** in acetonitrile (2% DMSO) with gradual addition of $CuCl_2$ (1×10^{-3} M) solution in acetonitrile. Concentration of **4** is 25 μM and highest concentration of $CuCl_2$ is 1.4×10^{-4} M. The spectra shows almost no change in CT band of **4** due to addition of Cu^{2+}. (B) UV-vis titration of **4** in presence of Cu^{2+} in acetonitrile (2% DMSO) with gradual addition of 4 μL TBAOH (1×10^{-3} M) solution in acetonitrile. Concentration of **4** is 25μM and Cu^{2+} is 12.5 μM. The spectra shows 51 nm red shift (Δλ) after achieving saturation with the addition of 1.2 equivalent of TBAOH.

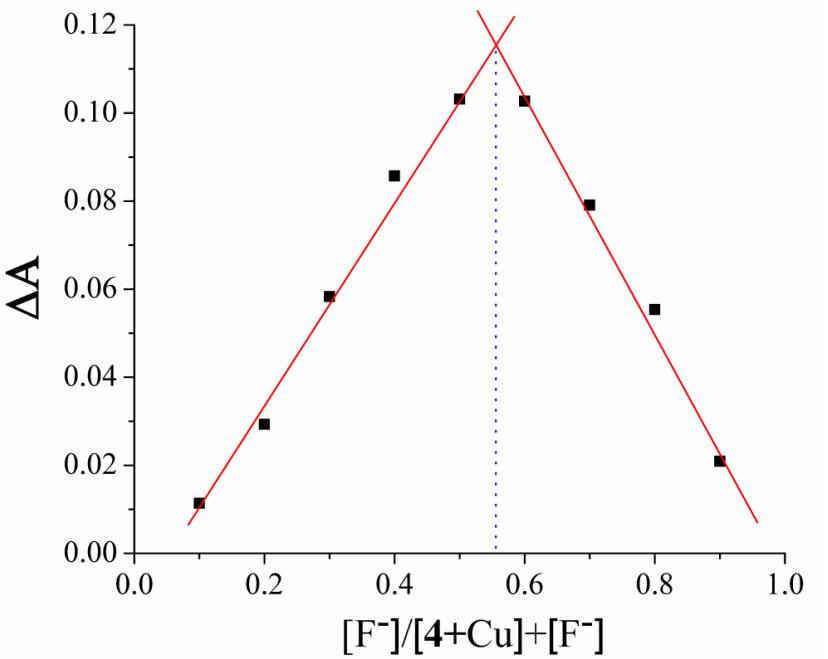

Fig. S17 Job's plot of binding of receptor **4** (25 μM) with fluoride in presence of Cu^{2+} (12.5 μM) where absorbance at 452 nm were plotted as a function of the molar ratio of **4**.

(A)

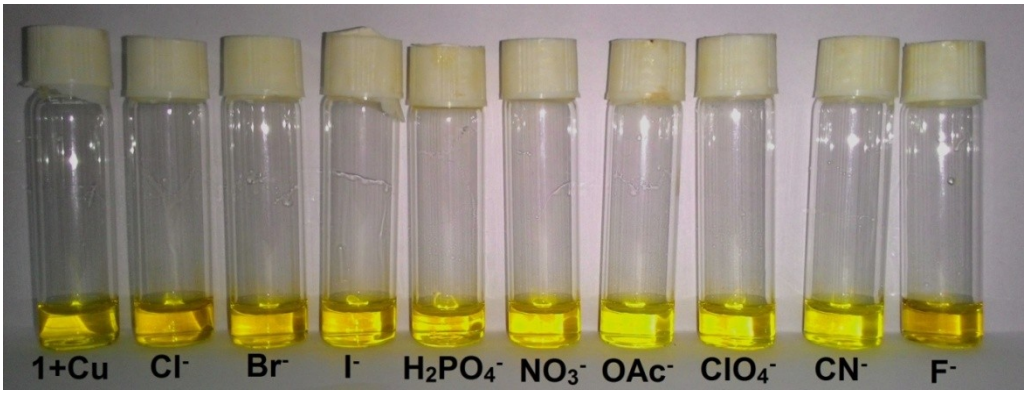

(B)

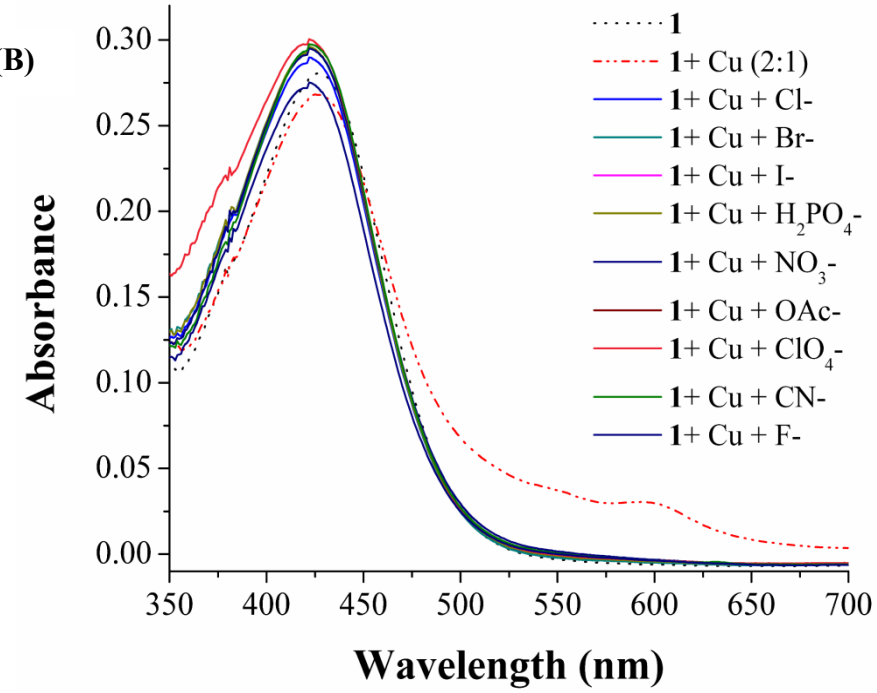

Fig. S18 (A) Colorimetric response of **1** (25 μM) in presence $CuCl_2$ (12.5 μM) with addition of different anions (1.5 X 10^{-4} M) in acetonitrile (2 % DMSO) solution. (B) UV-vis spectra of **1** (25 μM) in presence of $CuCl_2$ (12.5 μM) with addition of different anions (1.5 X 10^{-4} M) in acetonitrile (2 % DMSO) solution.

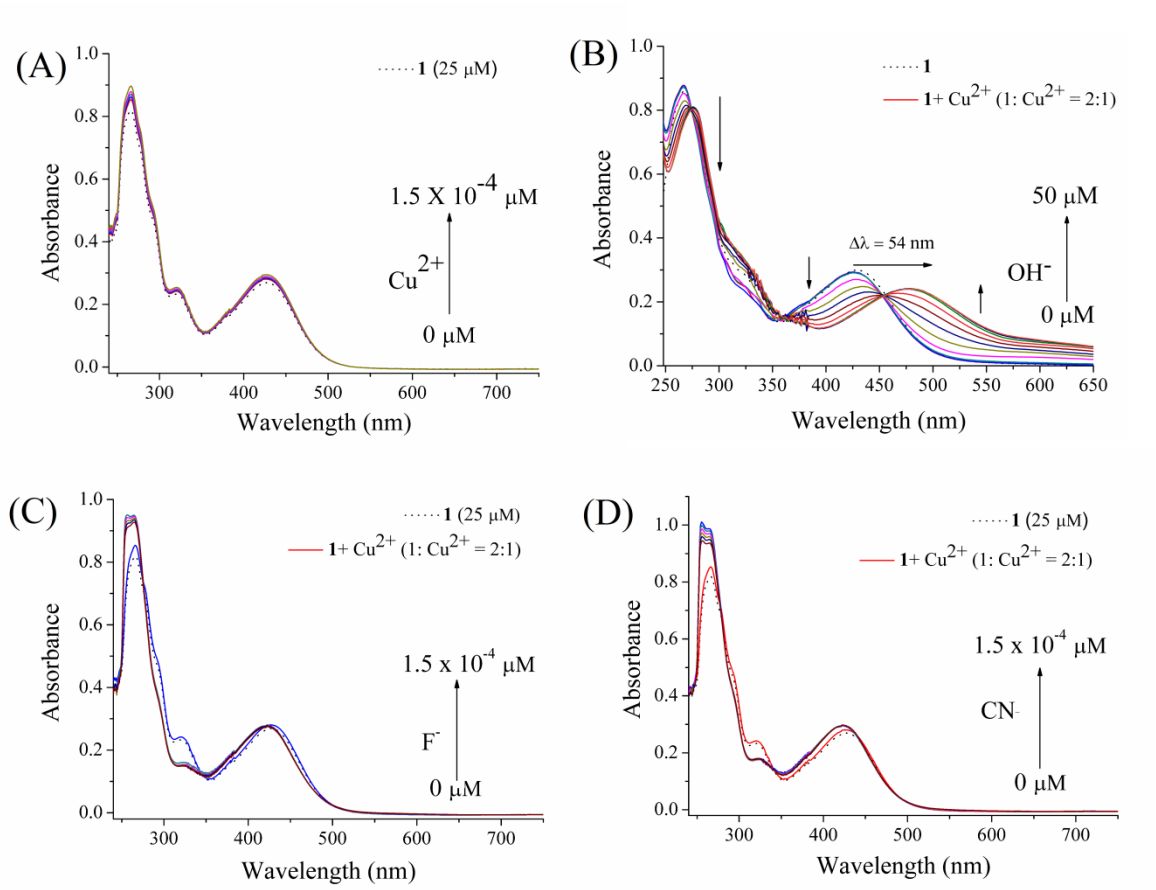

Fig. S19 (A) UV-vis titration of **1** in acetonitrile (2% DMSO) with gradual addition of $CuCl_2$ (1 × 10-3 M) solution in acetonitrile. Highest concentration of $CuCl_2$ is 1 × 10^{-3} M. The spectra shows no change in CT band of **1** due to addition of Cu^{2+} (B) UV-vis titration of **1** in presence of Cu^{2+} in acetonitrile (2% DMSO) with gradual addition of 4 μL TBAOH (1 × 10^{-3} M) solution in acetonitrile. Concentration of **1** is 25μM and Cu^{2+} is 12.5 μM. The spectra shows 54 nm red shift (Δλ) after achieving saturation with the addition of 2 equivalent of TBAOH. (C) UV-vis titration of **1** in acetonitrile (2% DMSO) in presence of Cu^{2+} (conc. 12.5 μM with gradual addition of TBAF (1 × 10^{-3} M) solution in acetonitrile. Highest concentration of F^- achieved is 1.5 × 10^{-4} M. The spectra showed almost no change in CT band of **1** due to addition of TBAF (D) UV-vis titration of **1** in acetonitrile (2% DMSO) in presence of Cu^{2+} (conc. 12.5 μM with gradual addition of TBACN (1 × 10^{-3} M) solution in acetonitrile. Highest concentration of F^- achieved is 1.5 × 10^{-4} M. The spectra showed almost no change in CT band of **1** due to addition of TBACN. The concentration of **1** in each case (A) to (D) is 25 μM.

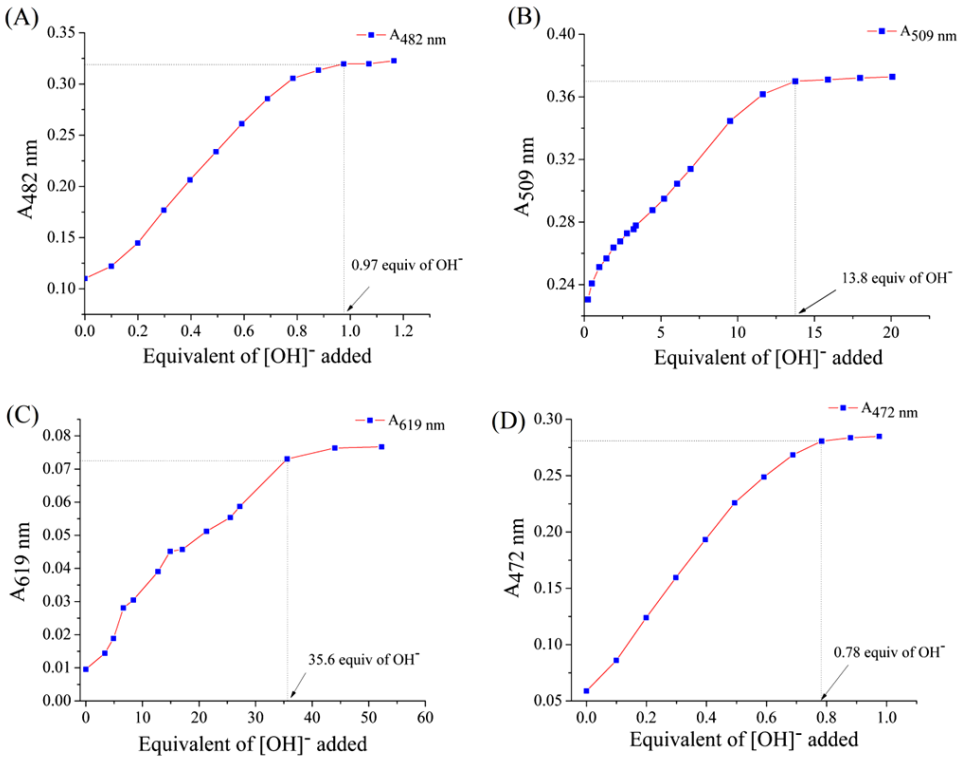

Fig. S20 UV-vis titration of (A) **1**, (B) **2**, (C) **3** and (D) **4** with gradual addition of TBAOH in acetonitrile medium (2% DMSO). The concentration of receptors in each case (A) to (D) is 25 μM.

Computational details

Theoretical calculations were done using Gaussian09 software package.[1] Optimisation of molecular structure has been performed at the DFT level of theory with B3LYP (Becke's three-parameter hybrid model using the Lee–Yang–Parr correlation functional) function[2, 3] and 6-31G(d) basis set. Ground state energies and oscillator strengths were computed based on B3LYP/6-31G(d) optimised geometries using TDDFT formalism in acetonitrile. The conductor-like polarizable continuum model (CPCM)[4, 5] was used with the acetonitrile as solvent in both optimisation and transition energy calculation. Electronic transitions, molecular orbital energies, electronic and related orbital contributions were extracted from output files using GaussSum 2.2 GUI application.[6] To assign the CT band shift with **1** and **4** we have used B3LYP function and 6-31G(d) basis set on the anion (deprotonating the benzimidazole moiety) of **1** and **4**.

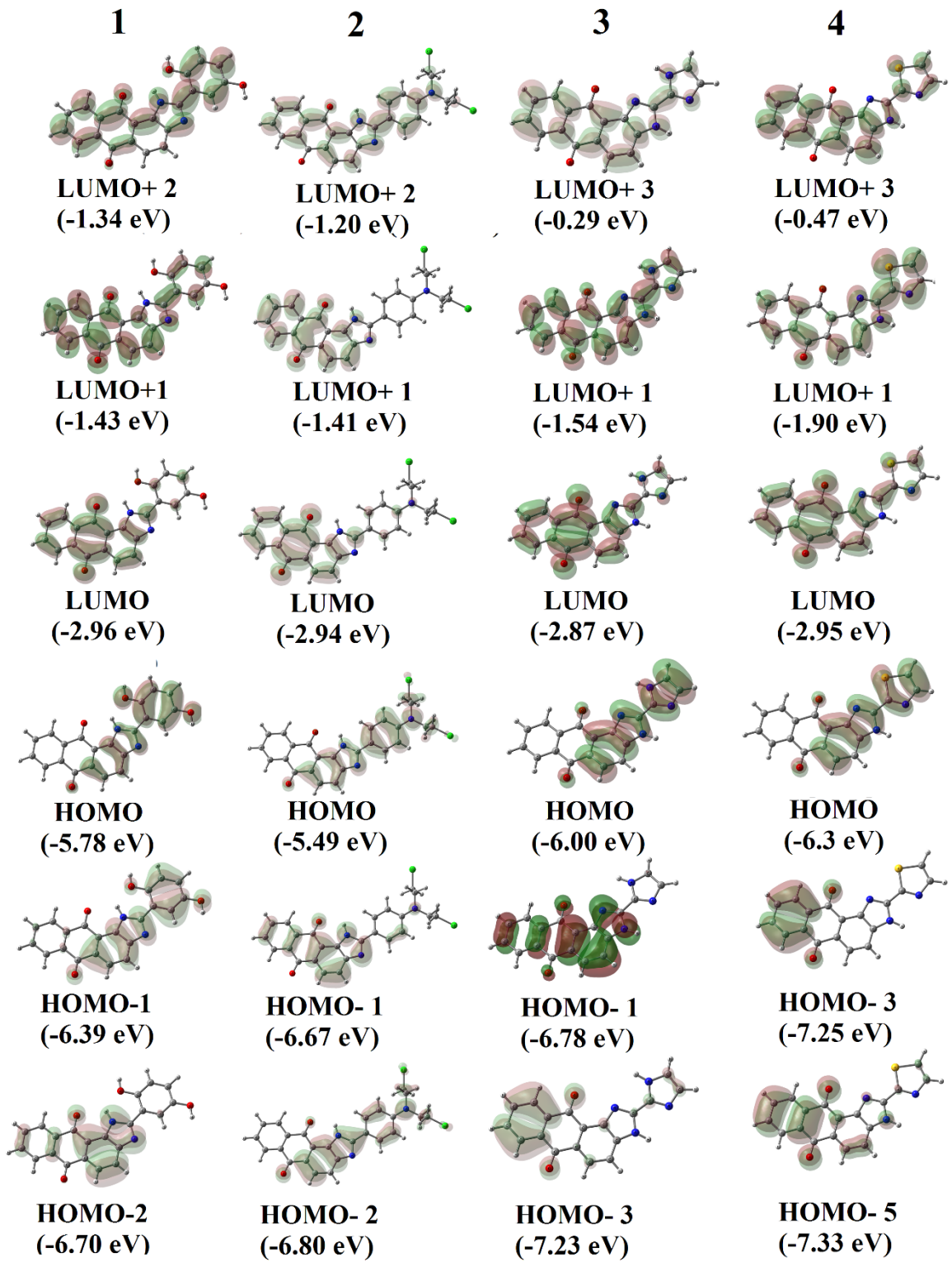

Fig. S21. Selected FMO illustrations and their respective energies (in eV) of ground state optimised geometry of **1-4** obtained from DFT level calculation at B3LYP/6-31G(d) in acetonitrile as solvent.

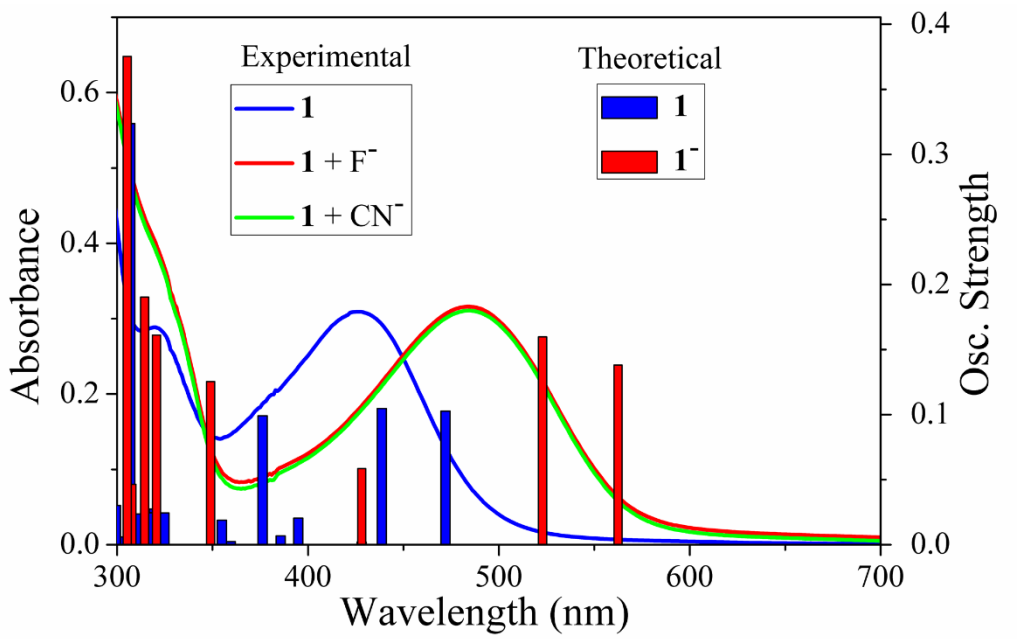

Fig. S22 A correlative spectral overlay of electronic transition of **1** in presence of anions (experimentally in line plot) in acetonitrile; Theoretically calculated transition of **1** and its benzimidazole –NH deprotonated species (**1**$^{-}$) using TDDFT at level of B3LYP/6-31G(d) in same solvent. Experimental data falls into the Gaussian distribution of calculated transitions (oscillation strength) showing good correlation.

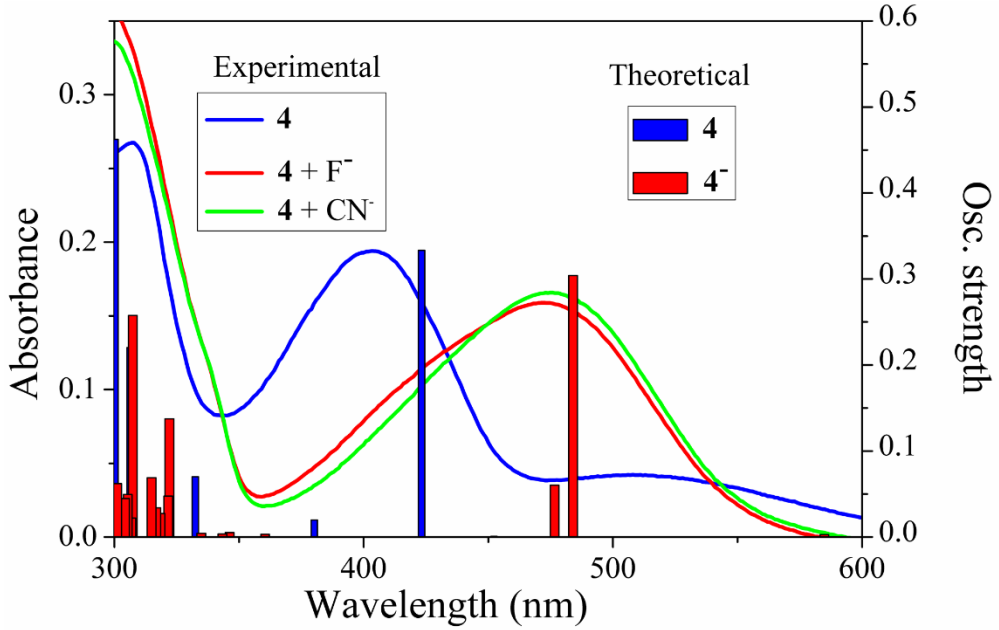

Fig. S23 A correlative spectral overlay of electronic transition of **4** in presence of anions (experimentally in line plot) in acetonitrile; Theoretically calculated transition of **4** and its benzimidazole –NH deprotonated species (**4**$^{-}$) using TDDFT at level of B3LYP/6-31G(d) in same solvent. Experimental data falls into the Gaussian distribution of calculated transitions (oscillation strength) showing good correlation.

Table S7. Selected electronic transition data obtained from TDDFT calculations using B3LYP/6-31G(d) and acetonitrile as solvent.

Sensor	λ_{Calc} (nm)	Osc. strength	Major MO contributions [a]
1	472	0.1026	HOMO(A) →L+2(A) (84%)
	439	0.1047	H-1(A) →LUMO(A) (11%), HOMO(B) →LUMO(B) (58%)
	376	0.0991	H-1(A) →LUMO(A) (15%), H-3(B) →LUMO(B)(23%), H-2(B)→LUMO(B)(16%), HOMO(B)→LUMO(B)(19%), HOMO(B) →L+1(B) (12%)
	307	0.3236	H-1(A) →LUMO(A) (28%), HOMO(B) →L+1(B) (43%)
2	555	0.4062	HOMO →LUMO (100%)
	400	0.0514	H-1 →LUMO (94%)
	365	0.0706	H-2 →LUMO(A) (92%)
	333	0.1278	HOMO →L+1(90%)
3	452	0.3262	HOMO →LUMO (98%),
	328	0.0753	H-3 →LUMO (88%)
	306	0.2883	HOMO →L+1 (88%)
4	423	0.3333	HOMO →LUMO (98%)
	332	0.0701	H-3 →LUMO (94%)
	306	0.2203	H-5 →LUMO (20%), HOMO →L+1(68%)

[a] Orbital contributions has been determined using GausSum 2.2 software package from Gaussian output file.

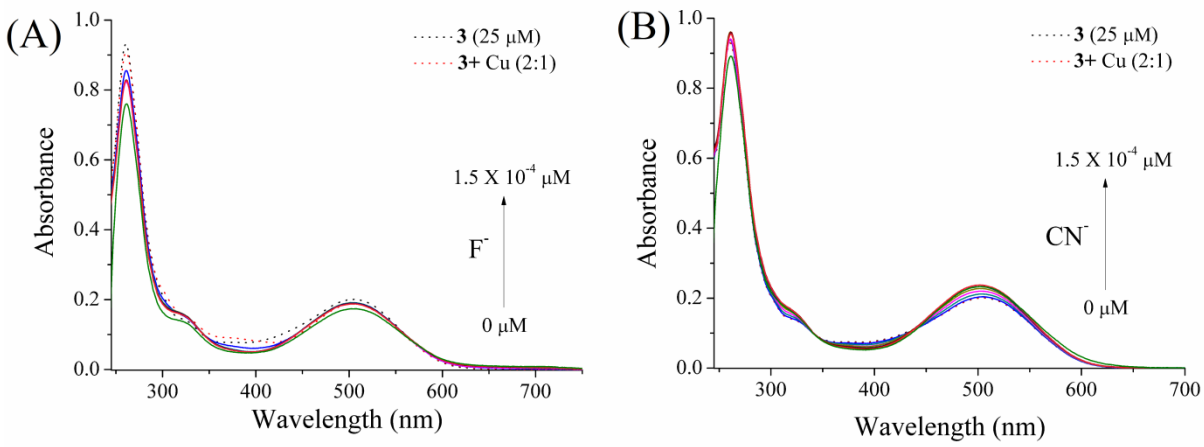

Fig. S24 (A) UV-vis titration of **3** in acetonitrile (2% DMSO) in presence of Cu^{2+} (conc. 12.5 μM with gradual addition of TBAF (1×10^{-3} M) solution in acetonitrile. Highest concentration of F^- achieved is 1.5×10^{-4} M. The spectra showed almost no change in CT band of **3** due to addition of TBAF (B) UV-vis titration of **3** in acetonitrile (2% DMSO) in presence of Cu^{2+} (conc. 12.5 μM with gradual addition of TBACN (1×10^{-3} M) solution in acetonitrile. Highest concentration of F^- achieved is 1.5×10^{-4} M. The spectra showed almost no change in CT band of **1** due to addition of TBACN. The concentration of **3** in each case (A) and (B) is 25 μM.

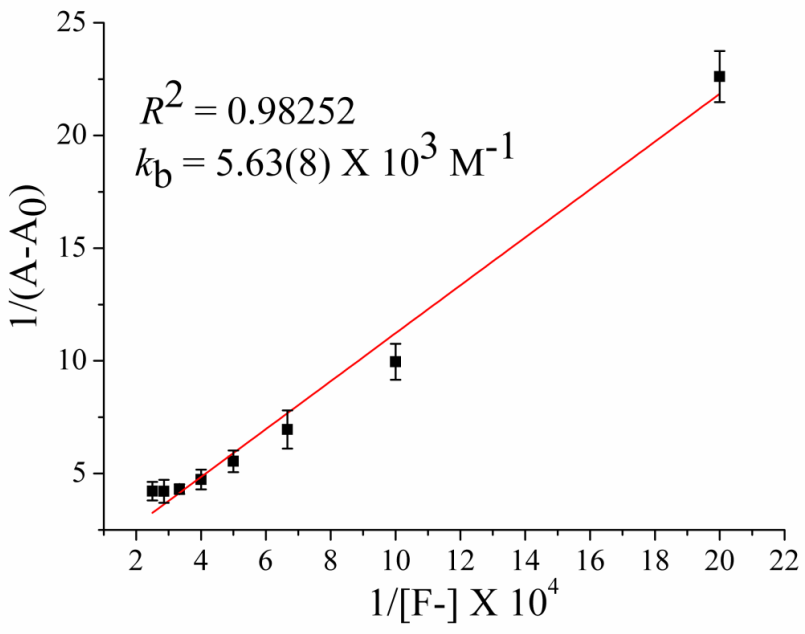

Fig. S25 Linear plot based on Benesi-Hildebrand equation for evaluation of binding constant of **1** with fluoride (0- 40 μM). Concentration of **1** is 25 μM.

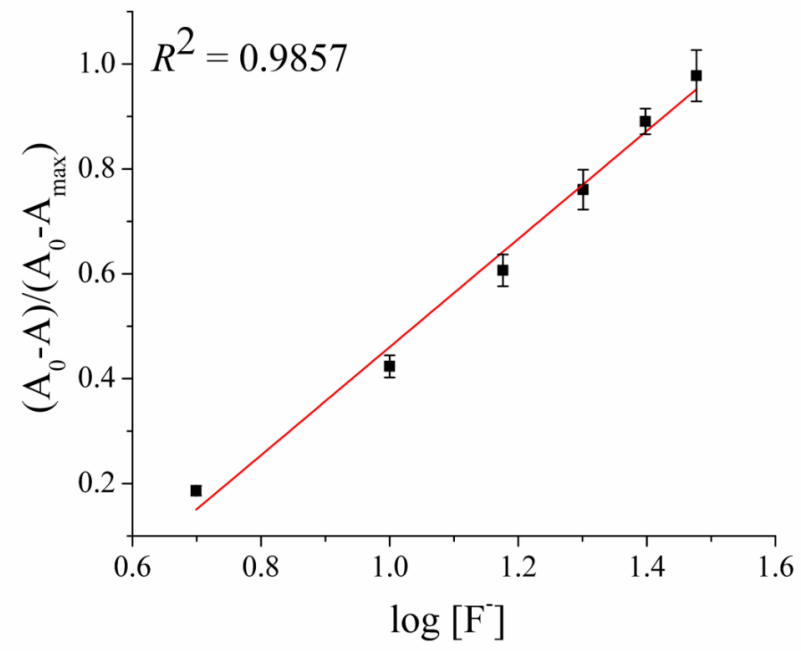

Fig. S26 A linear curve was obtained for the plot of $(A_0\text{-}A)/(A_0\text{-}A_{max})$ *vs.* log$[F]^-$. The intercept on the x-axis was considered as the detection limit. Thus the value obtained for the fluoride detection in case of **1** was found to be 3.57×10^{-6} (M). Concentration of **1** is 25 μM

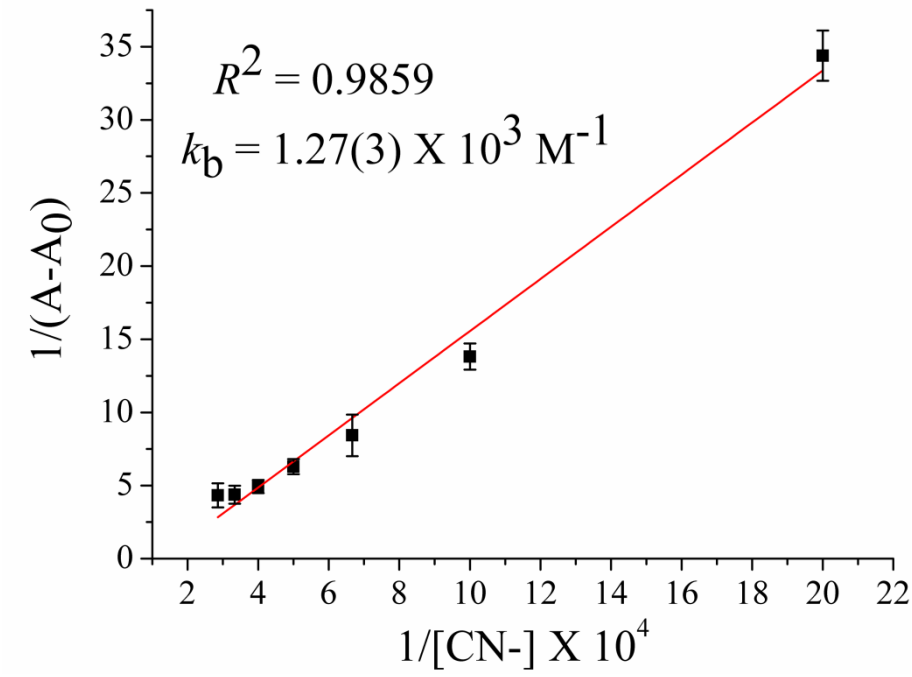

Fig. S27 Linear plot based on Benesi-Hildebrand equation for evaluation of binding constant of **1** with cyanide (0 - 35 μM). Concentration of **1** is 25 μM

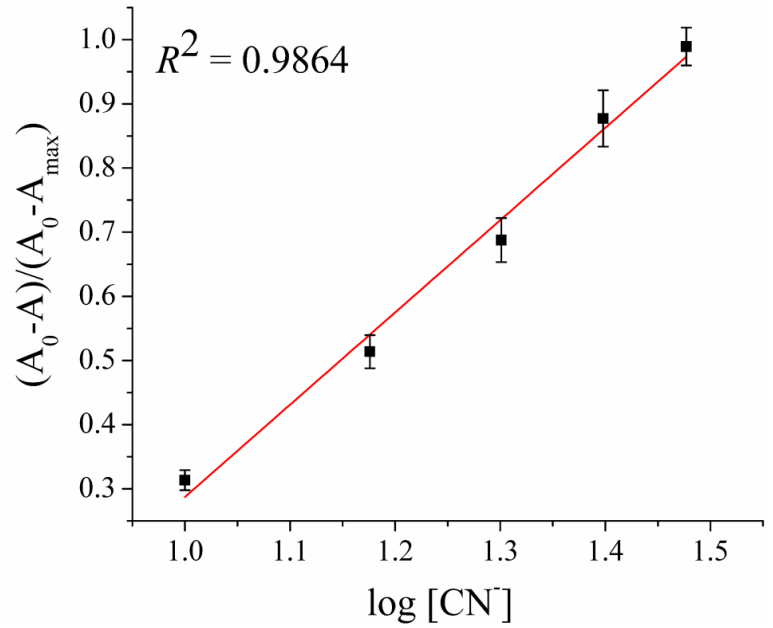

Fig. S28 A linear curve was obtained for the plot of $(A_0\text{-}A)/(A_0\text{-}A_{max})$ *vs.* log$[CN]^-$. The intercept on the x-axis was considered as the detection limit. Thus the value obtained for the cyanide detection in case of **1** was found to be 6.31×10^{-6} (M). Concentration of **1** is 25 µM

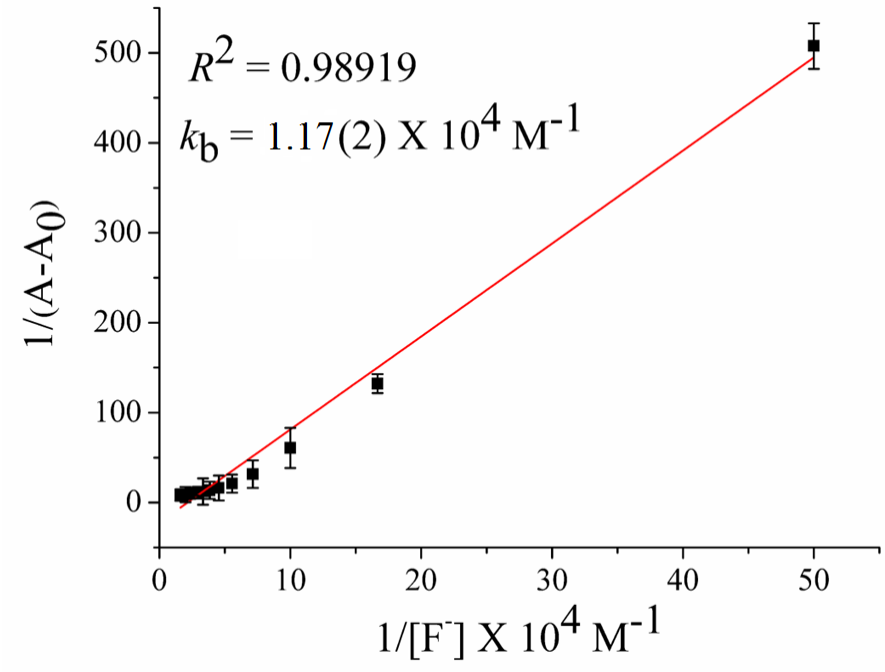

Fig. S29 Linear plot based on Benesi-Hildebrand equation for evaluation of binding constant of **4** with fluoride (0 - 62µM). Concentration of **4** is 25 µM

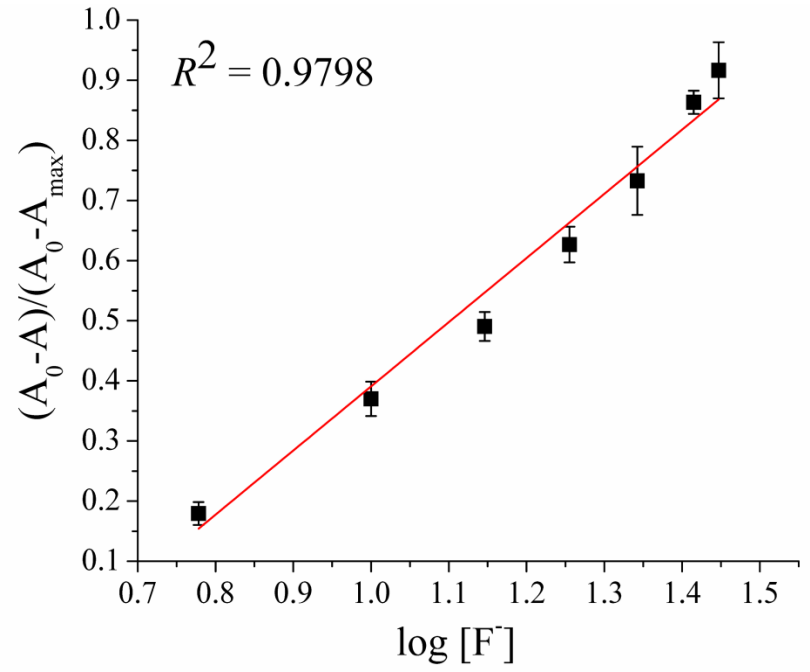

Fig. S30 A linear curve was obtained for the plot of $(A_0\text{-}A)/(A_0\text{-}A_{max})$ *vs.* log[F]$^-$. The intercept on the x-axis was considered as the detection limit. Thus the value obtained for the fluoride detection in case of **4** was found to be 4.30×10^{-6} (M). Concentration of **4** is 25 μM.

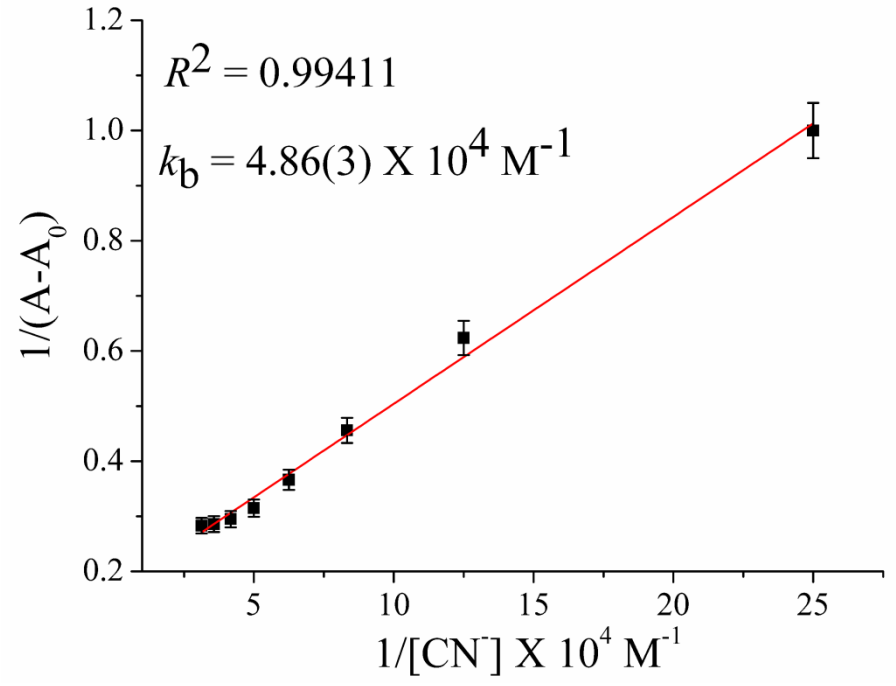

Fig. S31 Linear plot based on Benesi-Hildebrand equation for evaluation of binding constant of **4** with cyanide (0 - 32 μM). Concentration of **4** is 25 μM.

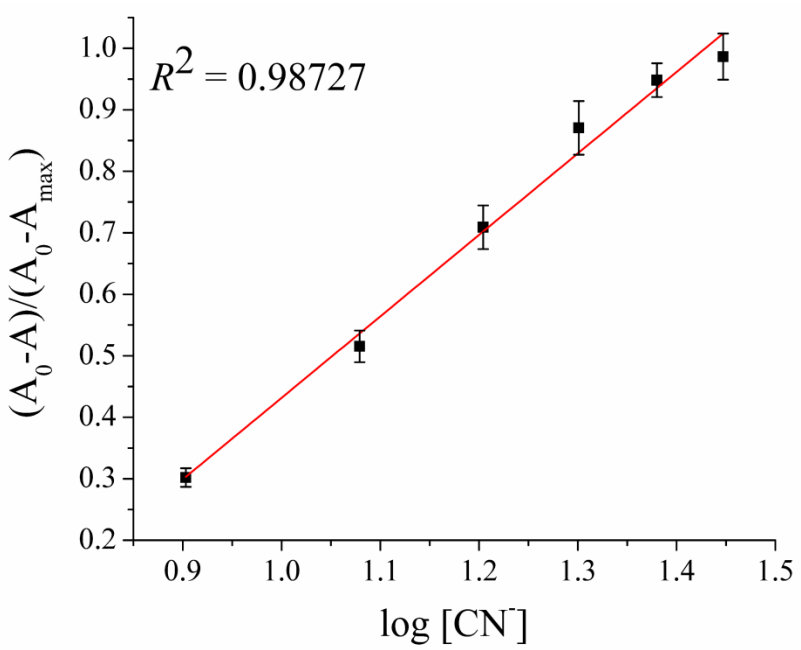

Fig. S32 A linear curve was obtained for the plot of $(A_0\text{-}A)/(A_0\text{-}A_{max})$ *vs.* log[CN]$^-$. The intercept on the x-axis was considered as the detection limit. Thus the value obtained for the cyanide detection in case of **4** was found to be 4.72×10^{-6} (M). Concentration of **4** is 25 μM

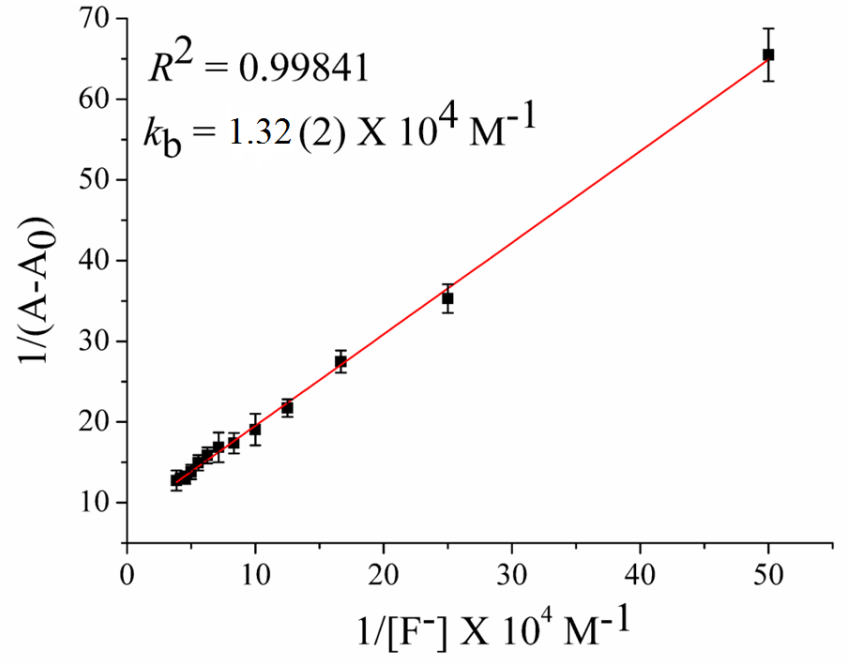

Fig. S33 Linear plot based on Benesi-Hildebrand equation for evaluation of binding constant of **4** (25 μM) in presence of Cu^{2+} (12.5 μM) with fluoride (0 - 26 μM).

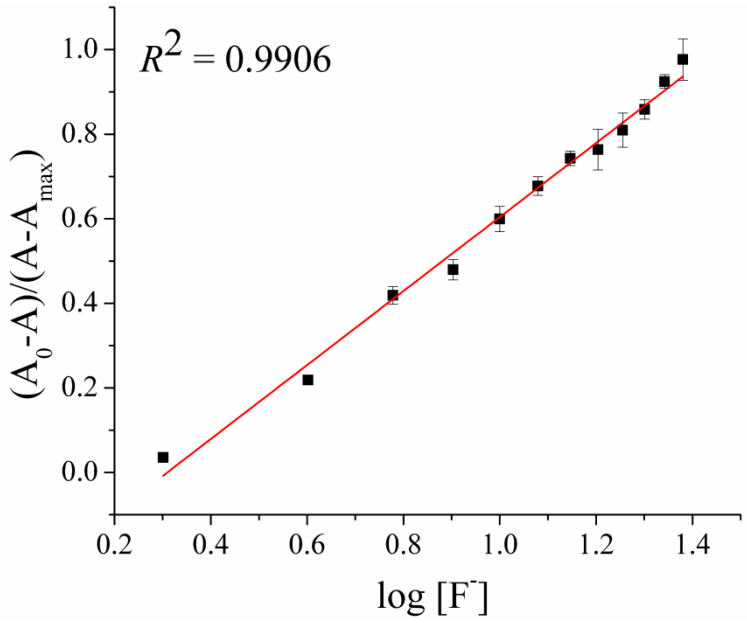

Fig. S34 A linear curve was obtained for the plot of $(A_0\text{-}A)/(A_0\text{-}A_{max})$ *vs.* log[F]$^-$. The intercept on the x-axis was considered as the detection limit. Thus the value obtained for the fluoride detection in case of **4** was found to be 2.03×10^{-6} (M). Concentration of **4** is 25 μM.

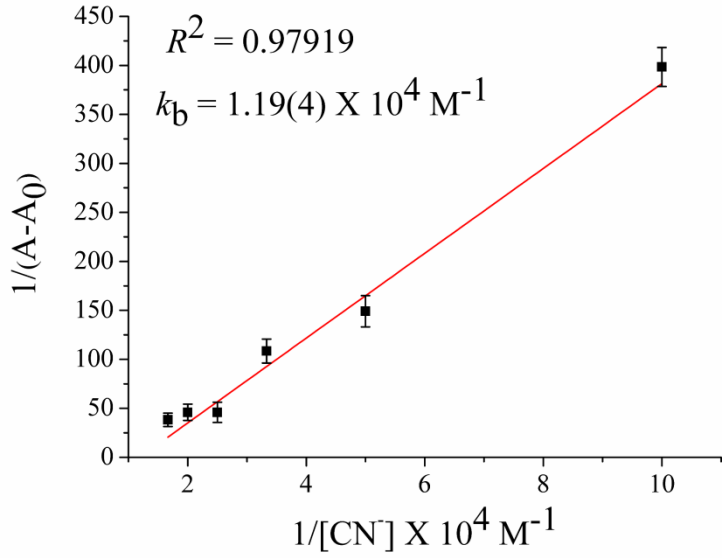

Fig. S35 Linear plot based on Benesi-Hildebrand equation for evaluation of binding constant of **4** (25 μM) in presence of Cu^{2+} (12.5 μM) with cyanide (0 - 60 μM).

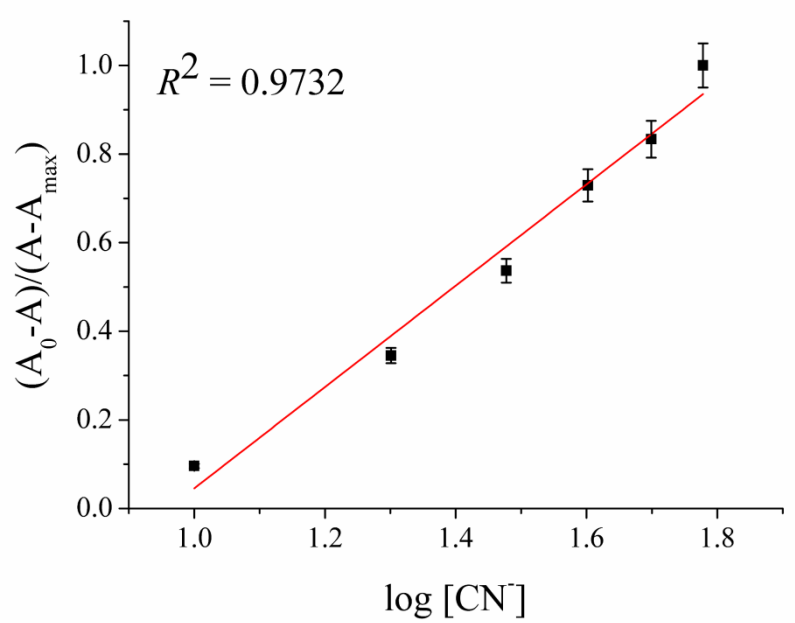

Fig. S36 A linear curve was obtained for the plot of $(A_0\text{-}A)/(A_0\text{-}A_{max})$ *vs.* log[CN]$^-$. The intercept on the x-axis was considered as the detection limit. Thus the value obtained for the cyanide detection in case of **4** in presence of Cu^{2+} was found to be 9.12×10^{-6} (M). Concentration of **4** is 25 μM.

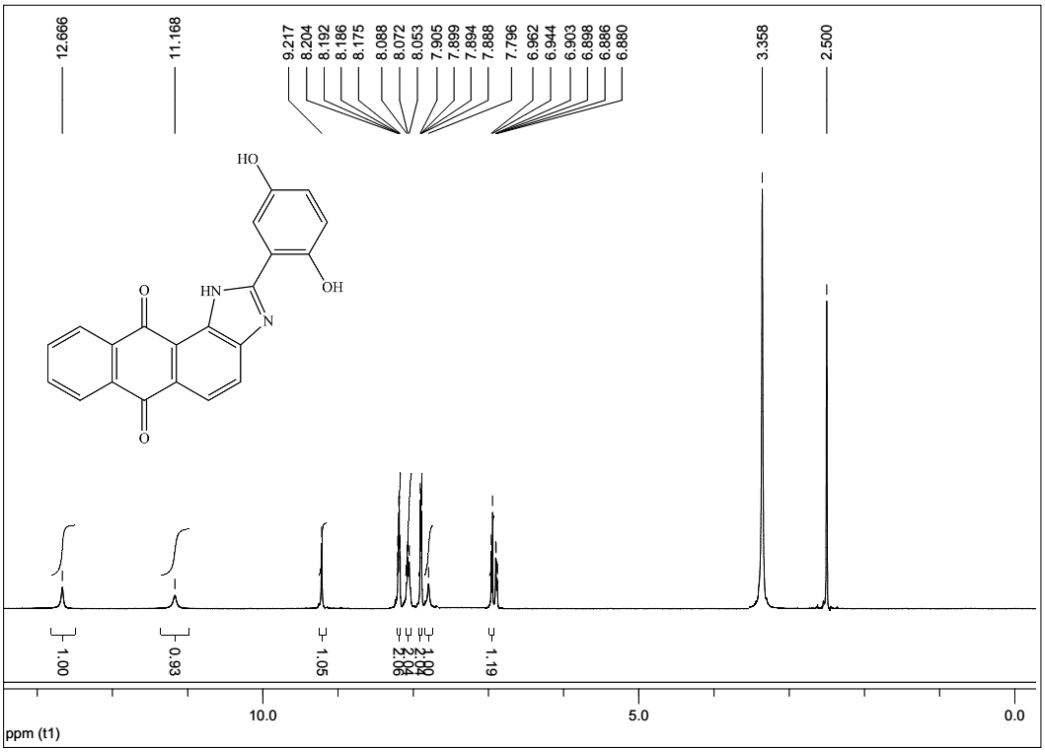

Fig. S37 ^{1}H NMR of **1** in DMSO-d_6.

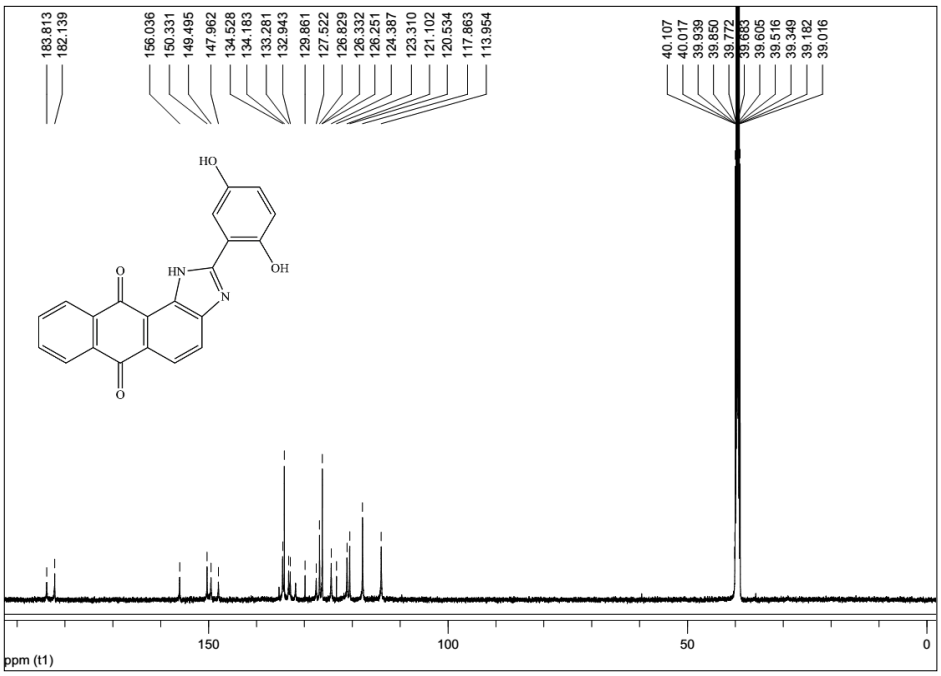

Fig. S38 ^{13}C NMR of **1** in DMSO-d_6.

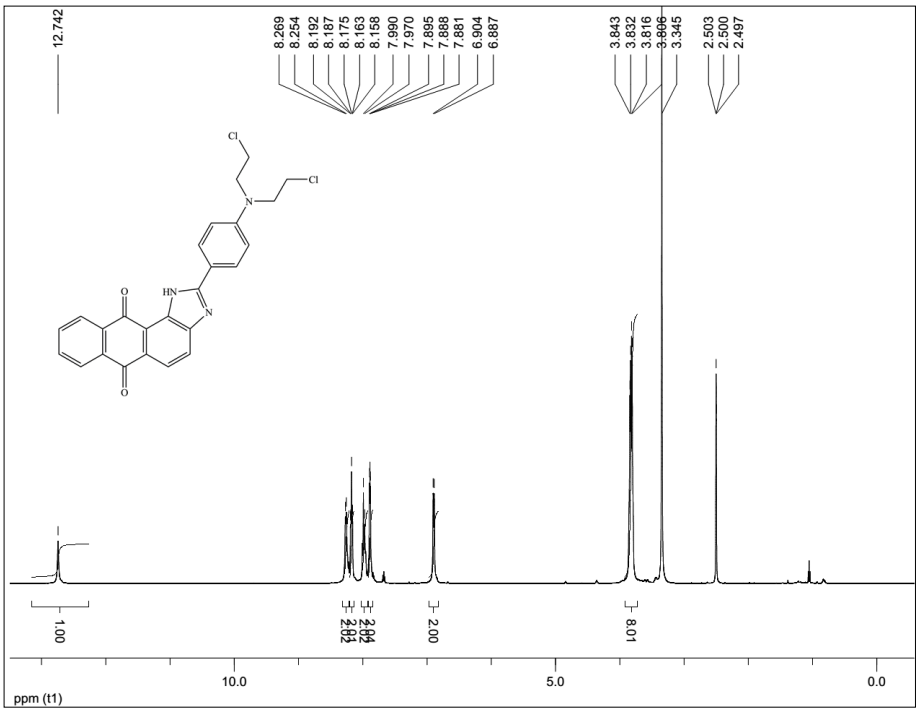

Fig. S39 ^{1}H NMR of **2** in DMSO-d_6.

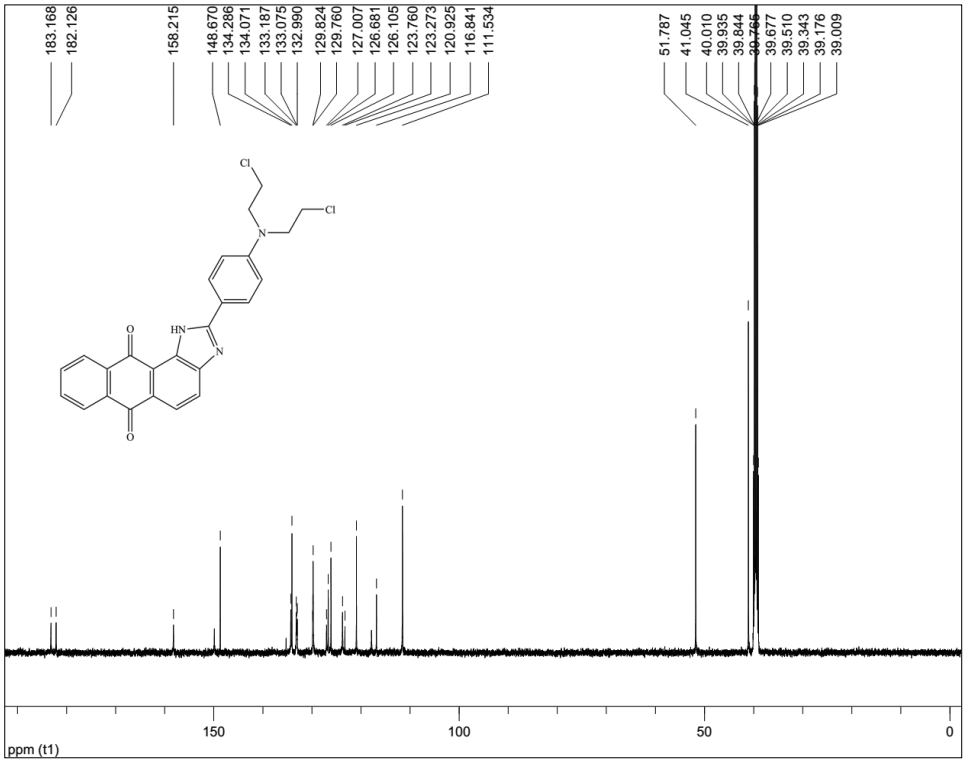

Fig. S40 ^{13}C NMR of **2** in DMSO-d_6.

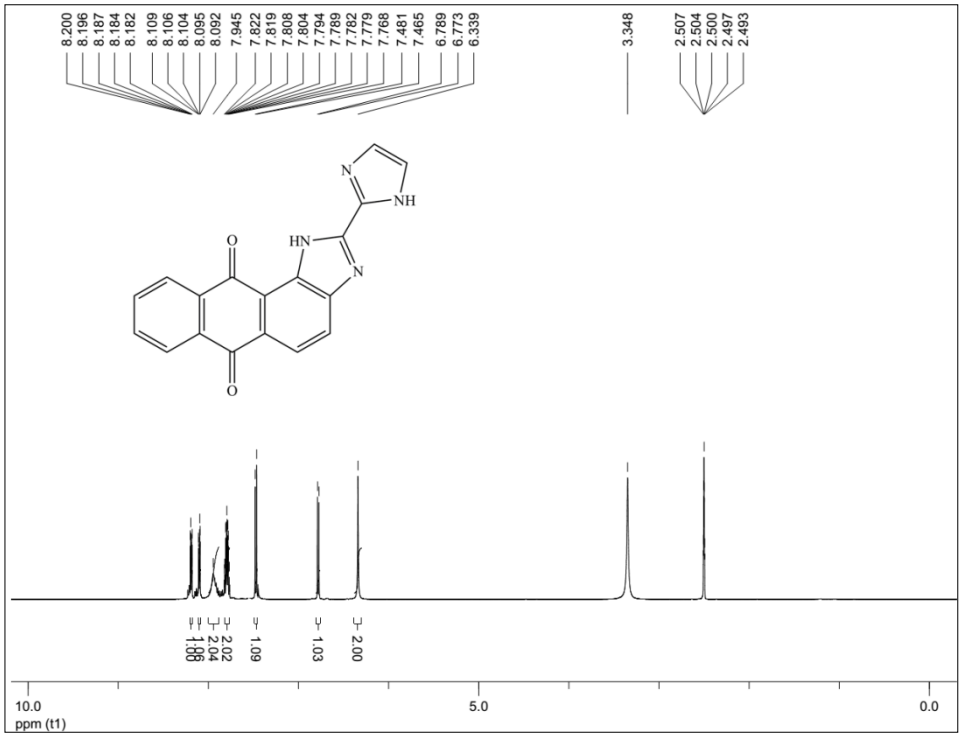

Fig. S41 ^{1}H NMR of **3** in DMSO-d_6.

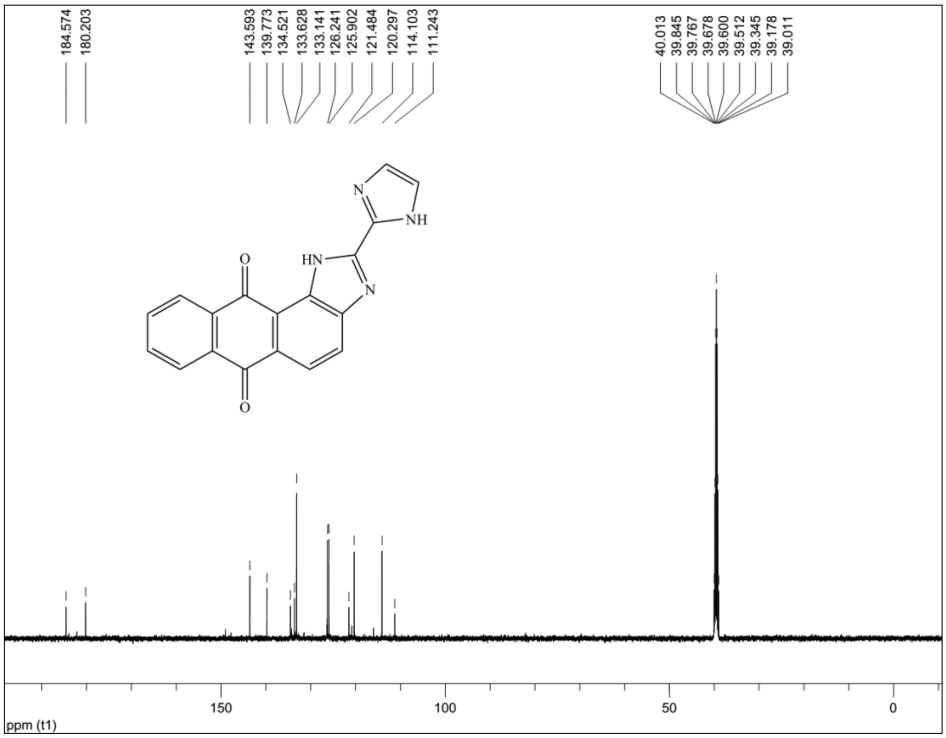

Fig. S42 ^{13}C NMR of **3** in DMSO-d_6.

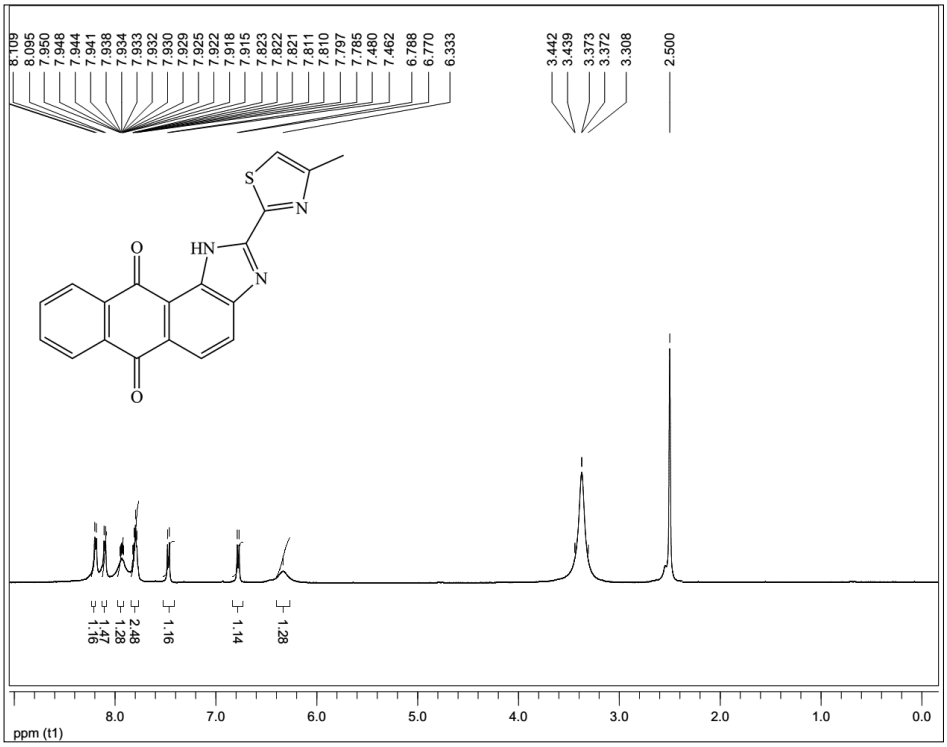

Fig. S43 ^{1}H NMR of **4** in DMSO-d_6.

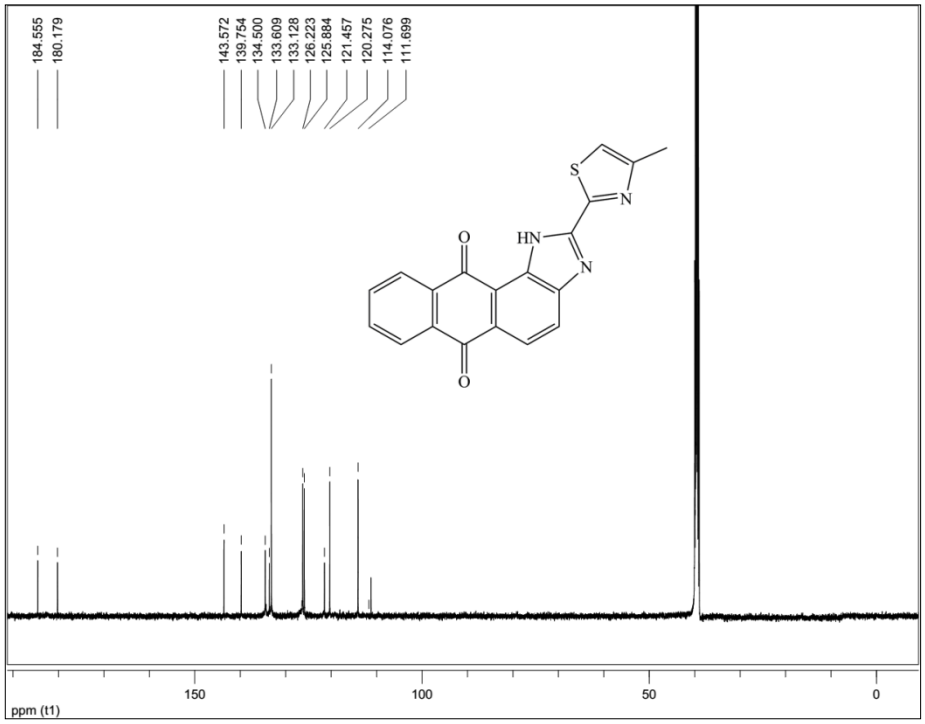

Fig. S44 ^{13}C NMR of **4** in DMSO-d_6.

References

1. M. J. Frisch, G. W. Trucks, H. B. Schlegel, G. E. Scuseria, M. A. Robb, J. R. Cheeseman, G. Scalmani, V. Barone, B. Mennucci, G. A. Petersson, H. Nakatsuji, M. Caricato, X. Li, H. P. Hratchian, A. F. Izmaylov, J. Bloino, G. Zheng, J. L. Sonnenberg, M. Hada, M. Ehara, K. Toyota, R. Fukuda, J. Hasegawa, M. Ishida, T. Nakajima, Y. Honda, O. Kitao, H. Nakai, T. Vreven, J. A. Montgomery Jr., J. E. Peralta, F. Ogliaro, M. J. Bearpark, J. Heyd, E. N. Brothers, K. N. Kudin, V. N. Staroverov, R. Kobayashi, J. Normand, K. Raghavachari, A. P. Rendell, J. C. Burant, S. S. Iyengar, J. Tomasi, M. Cossi, N. Rega, N. J. Millam, M. Klene, J. E. Knox, J. B. Cross, V. Bakken, C. Adamo, J. Jaramillo, R. Gomperts, R. E. Stratmann, O. Yazyev, A. J. Austin, R. Cammi, C. Pomelli, J. W. Ochterski, R. L. Martin, K. Morokuma, V. G. Zakrzewski, G. A. Voth, P. Salvador, J. J. Dannenberg, S. Dapprich, A. D. Daniels, Ö. Farkas, J. B. Foresman, J. V. Ortiz, J. Cioslowski and D. J. Fox, *Journal*, 2009.
2. C. Lee, W. Yang and R. G. Parr, *Phys. Rev. B: Condens. Matter Mater. Phys.*, 1988, **37**, 785-789.
3. A. D. Becke, *J. Chem. Phys.*, 1993, **98**, 5648-5652.
4. M. A. Aguilar and F. J. Olivares del Valle, *Chemical Physics*, 1989, **129**, 439-450.
5. A. A. Rashin and K. Namboodiri, *J. Phys. Chem.*, 1987, **91**, 6003-6012.
6. N. M. O'Boyle, A. L. Tenderholt and K. M. Langner, *J. Comput. Chem.*, 2008, **29**, 839-845.